Distribution Agreement

In presenting this thesis or dissertation as a partial fulfillment of the requirements for an advanced degree from Emory University, I hereby grant to Emory University and its agents the non-exclusive license to archive, make accessible, and display my thesis or dissertation in whole or in part in all forms of media, now or hereafter known, including display on the world wide web. I understand that I may select some access restrictions as part of the online submission of this thesis or dissertation. I retain all ownership rights to the copyright of the thesis or dissertation. I also retain the right to use in future works (such as articles or books) all or part of this thesis or dissertation.

_____ _____

Sung Bo (Joseph) Yoon Date

Subpopulation commensalism promotes Rac1-dependent invasion

of single cells via laminin-332

By

Sung Bo (Joseph) Yoon

Doctor of Philosophy

Graduate Division of Biological and Biomedical Sciences

Cancer Biology

Adam Marcus, Ph.D. Advisor	Sumin Kang, Ph.D. Committee Member
Jennifer Spangle, Ph.D. Committee Member	Mylin Torres, M.D. Committee Member
Wei Zhou, Ph.D. Committee Member	

Accepted:

Kimberly Jacob Arriola, Ph.D., MPH
Dean of the James T. Laney School of Graduate Studies

Date

Subpopulation commensalism promotes Rac1-dependent invasion of single cells via laminin-332

By

Sung Bo (Joseph) Yoon

B. S., Messiah University, 2017

Advisor:

Adam I. Marcus, Ph.D.

An abstract of a dissertation submitted to the Faculty of the

James T. Laney School of Graduate Studies of Emory University

in partial fulfillment of the requirements for the degree of

Doctor of Philosophy

in

Graduate Division of Biological and Biomedical Sciences

Cancer Biology

2024

Abstract

Subpopulation commensalism promotes Rac1-dependent invasion
of single cells via laminin-332

By Sung Bo (Joseph) Yoon

Phenotypic heterogeneity poses a significant hurdle for cancer treatment but is under-characterized in the context of tumor invasion. Amidst the range of phenotypic heterogeneity across solid tumor types, collectively-invading cells and single cells have been extensively characterized as independent modes of invasion, but their intercellular interactions have rarely been explored. Here, we isolate collectively-invading cells and single cells from the heterogeneous 4T1 cell line using Spatiotemporal Genomic and Cellular Analysis (SaGA) and observe distinct morphological differences between these subpopulations. Notably, collectively-invading cells exhibit prominent intercellular attachment mediated by E-cadherin, while single cells exclusively invade as detached individual cells. Furthermore, we observe extensive transcriptional and epigenetic diversity across these subpopulations. By integrating these datasets, we identify laminin-332 as a protein complex exclusively secreted by collectively-invading cells. Live cell imaging revealed that laminin-332 derived from collectively-invading cells increased the velocity and directionality of single cells. Despite collectively-invading and single cells having similar expression of the integrin α6β4 dimer, single cells demonstrated higher Rac1 activation upon laminin-332 binding to integrin α6β4. This mechanism suggests a novel commensal relationship between collectively-invading and single cells wherein collectively-invading cells promote the invasive potential of single cells through a laminin-332/Rac1 axis. To our knowledge, this finding represents the first characterization of a commensal interaction between cancer subpopulations wherein one subpopulation unilaterally provides a benefit to another subpopulation. The multi-omic workflow used to delineate this novel interaction can also be applied to other cancer subtypes to contribute towards a more comprehensive understanding of heterogeneous tumor dynamics.

Subpopulation commensalism promotes Rac1-dependent invasion of single cells via laminin-332

By

Sung Bo (Joseph) Yoon

B. S., Messiah University, 2017

Advisor:

Adam I. Marcus, Ph.D.

A dissertation submitted to the Faculty of the

James T. Laney School of Graduate Studies of Emory University

in partial fulfillment of the requirements for the degree of

Doctor of Philosophy

in

Graduate Division of Biological and Biomedical Sciences

Cancer Biology

2024

Table of Contents

List of Figures *(pages 50-65)*

Chapter 1: Introduction

1.1 – Cancer invasion and metastasis

1.1.1. Progress and outlook on breast cancer

Over the last several decades, cancer has remained the second leading cause of death in the United States (*1*). Specifically, breast cancer has remained the most prevalent cancer subtype in females, being responsible for 31% of estimated new cancer cases and 15% of estimated deaths in 2023 (*2*). Significant advances have been made towards early detection and treatment methods over the last 30 years, resulting in a 43% decline in breast cancer mortality since 1989, but incidence of invasive breast cancer rates have steadily been increasing about 0.5% per year (*1, 2*). These statistics reveal the tremendous impact scientific research has had on breast cancer patient outcomes, while illuminating the need to more holistically understand and target this ever-evolving disease.

Amidst the significant advances made in detecting and treating local breast tumors, metastatic breast cancer—along with other metastatic cancer subtypes— remains largely incurable (*3*). This incurability stems largely from the heterogeneity of primary tumors contributing towards metastases at secondary sites with distinct transcriptional and epigenetic profiles (*4*). The potential for such diverse metastases emerging from a single tumor results in the ineffectiveness of targeted therapeutics and the clinical dependency towards debilitating systemic chemotherapy (*4, 5*). In an effort to curb the inevitability of metastatic disease, recent efforts have focused on tempering the ability of cancer cells to invade and metastasize. Such efforts have resulted in the development of therapies targeting genes crucial to the metastatic cascade, including denosumab—a humanized monoclonal antibody targeting the receptor activator of NF-

κB ligand—and cilengitide—a peptide inhibitor αvβ3 and αvβ5 integrins—but both therapies resulted in either negative clinical trials or discontinuation of use to target metastatic disease (*5*). These therapeutical incompatibilities represent the urgent need to discover novel strategies to inhibit metastatic progression.

1.1.2. The metastatic cascade

Despite being responsible for 90% of cancer-related deaths, regulation of metastasic processes remains poorly understood (*6*). Metastasis can be described as a multicellular response of cancer cells to nutritional and spatial restriction. The unnatural proliferation of a tumor presents physical constraints to the tumor itself as it continues to grow beyond the borders of the surrounding stroma *(4, 6)*. Additionally, proliferating tumors require exponentially more nutrients than healthy tissue, resulting in the emergence of cells that do not depend on the primary tumor for survival, but are able to mobilize to attain the necessary nutrients to continue surviving and proliferating (*7*). These demands push cancer cells to undergo multiple genetic and transcriptional transformations to adapt to the obstacles the body presents to halt such malignant dissemination (*6*).

The metastatic cascade begins with the selective pressures a highly proliferative tumor presents. As tumors grow over 1 cm^3 in volume, the number of cancer cells requiring oxygen outpaces the rate at which new blood vessels sprout, resulting in a hypoxic—low oxygen—environment for the cancer cells in the center of the tumor (*8*). Cancer cells within a hypoxic environment react by inducing expression of the HIF1α transcription factor, which in turn results in the secretion of VEGF (vascular endothelial growth factor) into the surrounding stroma (*9,*

10). Secreted VEGF binds to VEGF receptors in local endothelial cells, which stimulates angiogenesis—the budding of nascent blood vessels from pre-existing blood vessels. Specifically, VEGF receptor activation through VEGF binding in endothelial cells stimulates both proliferation and migratory capabilities to guide the emerging blood vessel towards the VEGF-secreting cells (*11*). Nascent endothelial cells are guided by leading "tip" cells through VEGF-directed chemotaxis until they reach the cancer cells to supply oxygen and nutrients (*11, 12*). In addition to providing the necessary nutrients for cell survival, nascent vasculature provides a direct route for hypoxic cancer cells to escape the nutrient scarce environment that a growing tumor presents (*13, 14*). From being physically restricted by nearby cells and often highly dense stroma, angiogenesis offers cancer cells a secondary route towards survival.

Despite the availability of nascent vasculature, cancer cells still face multiple physical obstacles that need to be overcome to enter into the bloodstream. To start, cancer cells must overcome basement membranes that surround the tumor itself and line blood vessels. Basement membranes are dense linings composed predominantly of laminins and non-fibrillar collagens and usually delineate flexible boundaries for healthy tissue (*15*). To penetrate this basement membrane, cancer cells develop capabilities to break down these extracellular matrix proteins, namely through the secretion of matrix metalloproteases (MMP) (*16*). Breakdown of this basement membrane enables the local dissemination of cancer cells to nearby tissues and initiates the spread of cancer cells to distant organs via the bloodstream (*15, 16*). To spread, proliferative cancer cells activate cell motility mechanisms, enabling them to move through dense stromal environments. The invasive modalities that cancer cells adopt to move will be further detailed below. In addition to these processes, cancer cells must also contend with the inflammatory response mounted against these cells upon breach of basement membrane

components and heightened hypoxic and angiogenic conditions in the primary tumor (*17*). In response to these pressures, cancer cells evolve to evade the immune system via aberrant degradation of MHC molecules and expression of immune checkpoint molecules to hide from natural killer cells and cytotoxic T cells (*18, 19*).

While in circulation, cancer cells experience further selective pressures, including stress induced by high shear forces and anoikis—cell death induced from the detachment to solid substrates (*20*). Additionally, cancer cells in circulation are more vulnerable to immune attack due to the abundance of circulating surveillance immune cells (*20*). Due to these extrinsic and intrinsic pressures, the majority of cancer cells that enter the circulation do not survive, but a few rare cells that have evolved anoikis resistance and immune evasion mechanisms can maneuver past blood vessels at distant organs (*i.e.* extravasation) and invade into a secondary site (*21*). Implantation of cancer cells into a secondary site does not always guarantee the formation of another mass as small clusters of cells can stay dormant for multiple years and remain largely undetectable (*i.e.* micrometastases) (*22, 23*). Among these micrometastases, some could develop capabilities to grow into proliferative masses (*i.e.* macrometastases) and cause significant damage to the secondary organ site in which it is embedded (*21*).

Due to the complex multi-step nature of metastasis, it is a highly inefficient process for individual cancer cells. As such, metastasis is a highly vulnerable process that is largely curtailed by the innate and adaptive defenses posed by the human body. Despite this, efforts to prevent and treat metastatic disease have proved futile (*5*), further illuminating the urgent need to more comprehensively understand the underpinnings and regulatory mechanisms of metastatic disease.

1.1.3. Collective cell invasion

Among the numerous potential therapeutic targets for metastasis, the vast majority of targets involve cancer cell invasion (*5*). Despite this, effective targeting of invasive cancer cells has proved challenging due to the vast spectrum of distinct invasive phenotypes cancer cells employ (*24*). The majority of these modalities fall within two broad categories of cell invasion: collective and single-cell invasion.

Collective invasion is characterized as invasive cells moving in adhered groups, frequently forming a chain of connected cells (*24*). The ability for cells to move collectively is not unique to cancer cells. In particular, healthy endothelial cells proliferate and move collectively during angiogenesis to generate nascent blood vessels in response to VEGF signaling, and various cell types move collectively during embryogenesis to reach distant sites or form complex organ shapes (*11, 25*). To move collectively, cells upregulate a variety of cell-cell junction proteins, including E-cadherin and N-cadherin, while sequentially activating both Rho and Rac GTPases for actomyosin contractility (*24*). Collective movement also often entails the emergence of a leading "tip" cell and following "stalk" cells, as is classically termed from branching morphogenesis during nascent blood vessel formation (*11*). The spatial polarity of "tip" and "stalk" cells also represents a polarity in phenotypic attributes, namely in the elevated secretion of MMPs and increased formation of filopodia within the "tip" cells to help navigate and eventually penetrate dense stromal barriers (*11*, *12*).

Cancer cells adopt these intrinsic mechanisms to invade collectively, and as a result collective invasion is observed in the majority of solid tumor types and represents the predominant mode of invasion in these solid tumors (*26*). In lung cancer, distinct "leader" and "follower" subpopulations within collective chains have been shown to cooperate to invade

through dense matrices and abrogation of this heterogeneity restricted the ability for these cells to invade collectively (*27*). In particular, leader cells in lung cancer cells have been shown to drive collective invasion through robust filopodial extensions and fibronectin micropatterning, while follower cells secrete growth factors to support leader cell survival (*27, 28*). Despite existing together in a collective pack, leader and follower cells exhibit significant transcriptional differences and mutually exclusive metabolic dependencies that together enable more resilient and efficient cancer cell invasion (*28, 29*). In contrast, leader and follower cells in breast cancer are less phenotypically distinct, as these metabolically-distinct subpopulations have been shown to alternate in leading collective chains (*30*). Instead, the co-existence of cells invading as collective packs and as single cells within the same tumor has been of recent interest within metastatic breast cancer, as further detailed below.

Cancer cells invading collectively have higher tendencies to circulate in the bloodstream as clusters of cells (*31*). Relative to single cells, circulating tumor clusters have demonstrated the ability to form metastatic sites more robustly, suggesting that clustering presents a metastatic advantage to cancer cells compared to individualization (*32*). Multiple reasons have been uncovered for the metastatic advantage to clustering, including increased resilience against cell death imposed by high shear forces in the bloodstream and elevated anoikis resistance due to the persistence of cell-cell junctions like E-cadherin while circulating cells are clustered (*32, 33*). Additionally, circulating tumor clusters have shown higher immune evasion capabilities, notably through binding to platelets and myeloid-derived suppressor cells which act as shields against immune surveillance (*34, 35*). Due to these advantages, quantification of circulating tumor clusters versus circulating tumor single cells in both breast and prostate cancer patient blood samples showed a significantly higher percentage of clustered cancer cells (*32*). These findings

suggest that collective invasion enables more robust metastatic disease in multiple solid tumor types.

1.1.4. Single cell invasion

Single cell invasion is characterized as invasive cells moving independently of cell-cell adhesions (*24*). Single cell invasion is most common in tumors wherein the host tissue is not predominantly epithelial, including tumors in connective tissue and immune malignancies (*24*). Relative to collective invasion, single cell invasion is broadly considered more stochastic in nature due to the absence of any physical restraints posed by cell-cell interactions. Like collective cell movement, single cell movement is not unique to cancer or other disease states. Within the healthy human body, single cell movement is most prominently observed in the vast majority of immune cells, which often need to penetrate dense matrices and cell-cell barriers such as endothelial linings to reach damaged tissue (*36*). In particular, two predominant modes of single cell movement have been demonstrated: mesenchymal and amoeboid single cell movement.

Mesenchymal single cell movement is characterized as individual cells that rely on actomyosin contractility and filopodial extrusions to penetrate dense stromal matrices (*24*). Like collectively-invading cells, mesenchymal cells activate Rho and Rac GTPases to generate traction forces via actomyosin contractility and form new focal adhesions by integrin binding (*37*). Despite the absence of cell-cell adhesions with other nearby cells, mesenchymal cells display highly directional movement (*38*). The flexibility offered by the increased surface area provided by the absence of direct intercellular adhesions allows for high cell velocities for

mesenchymal cells (*24*). Mesenchymal cells also express and secrete MMPs from filopodial extrusions to break down ECM components and also have capabilities for ECM remodeling (*39, 40*). Furthermore, inhibition of MMP secretion or Rho activation have been sufficient to abrogate mesenchymal invasion, revealing the importance of these pathways for maintenance of the mesenchymal phenotype (*41, 42*).

In direct contrast to mesenchymal movement, amoeboid single cell movement is characterized as individual cells that do not depend on generating traction forces or secretion of extracellular proteases to move (*24*). Instead, amoeboid cells have highly plastic cell morphologies and low adhesion of collagen and other ECM substrates, allowing for efficient maneuvering through tight spaces (*24*). In the human body, most lymphocytes move using amoeboid-like movement through "gliding" motions consisting of short-lived and weak cell-substrate interactions (*24*, *43*). In contrast to stress fibers that mesenchymal cells use to propel forward and form focal adhesion sites, amoeboid cells depend on force generated from cortical filamentous actin to adapt to their surrounding substrates (*43, 44*). Due to these characteristics, amoeboid invasion allows for the most rapid and efficient mode of dissemination from a primary tumor among invasive modalities, often resulting in early lymphatic and metastatic spread (*45, 46*).

1.1.5. Plasticity between invasion modalities

A distinct hallmark of cancer cells is their ability to adapt to different environments and selective pressures (*47*). To adapt, cancer cells can transition between distinct phenotypes to

promote survival, and effective navigation and penetration of a diverse range of stromal components.

Among these phenotypic transitions, epithelial-to-mesenchymal transition (EMT) is the most well characterized. Cells in tissues of epithelial origin express high levels of cell-cell adhesion proteins, including E-cadherin, claudins, and ALCAM, all of which allow for retention of intercellular adhesion and distinct apical-basal cell polarity (*48*). As epithelial cells become anaplastic, some cells lose these epithelial markers to allow for cell movement in response to nutritional scarcity and oxygen depletion (*48*). In particular, secreted VEGF from angiogenic blood vessels activates EMT transcription factors, such as Snail, Slug, and Twist, which in turn upregulates expression of proteins that support cell movement including vimentin and fibronectin (*49*). Through EMT, cells acquire the ability to form filopodial extrusions and lose apical-basal cell polarity, resulting in spindle-like morphology and cell individualization (*48, 49*). Despite the seemingly linear nature of EMT, recent work has established a great appreciation for partial EMT states that exist within the EMT spectrum, including cancer cells that have simultaneous expression of both epithelial and mesenchymal markers (*50, 51*). Collectively-invading cells are considered to exhibit one of these partial states due to the concomitant presence of cell-cell junction proteins and filopodia-dependent cell movement (*52*).

Mesenchymal cells can also transition into amoeboid cells through mesenchymal-to-amoeboid transition (MAT). MAT is observed most commonly in response to therapeutic agents that target proteins involved in filopodia-dependent cell movement, including MMPs and focal adhesion kinase (*46, 53*). Through activation of Rho and ROCK GTPases, mesenchymal cells can reduce their dependency to these mechanisms for cell motility, reducing the efficacy of these therapies (*54*). In addition to external pressures, lysophosphatidic acid, Met overexpression, and

cytokines secreted from tumor-associated macrophages have also induced MAT in multiple cancer cell lines (*53*). The process of epithelial cells becoming amoeboid cells through both EMT and MAT has also been implicated with increased dedifferentiation, with cells undergoing MAT in particular being associated with increased stemness (*24, 55*). Much still remains undiscovered regarding the clinical applications of inhibiting MAT, although like EMT, the existence of heterogeneous partial states within MAT is likely.

In addition to EMT and MAT, reverse transitions have also been observed in cancer cells, albeit being less prevalent. Mesenchymal-to-epithelial transition (MET) has been observed at metastatic sites in particular, where motile and morphologically flexible cells colonize and begin proliferating at the secondary site by adopting an epithelial phenotype (*56*). Interestingly, a unique subset of myeloid cells have been shown to secrete the proteoglycan versican to induce MET in lung metastases by suppressing Smad2 (*57*). Additionally, lineage labeling experiments in pancreatic adenocarcinoma have found circulating tumor cells (CTCs) expressing E-cadherin, suggesting that MET can also occur while cancer cells are in circulation (*58*). Additionally, amoeboid-to-mesenchymal transition (AMT) has been found to be induced by ERK activation through TGF-β1 in oral squamous cell carcinoma (*59*). In this model, AMT was found to be actively repressed by cofilin-1 expression to maintain the amoeboid phenotype, suggesting that amoeboid cells have high phenotypic persistence (*59*).

In all, cancer cells are highly adaptable and can transition between transcriptional cell states to optimize their survival and motility. This flexibility poses a significant roadblock for cancer treatment, highlighting the importance of better understanding the basis for these diverse cell states and the mechanistic underpinnings of these phenotypic transitions.

1.2 – Subpopulation interactions and dynamics

1.2.1. The genomic and epigenomic basis for phenotypic heterogeneity

The long-term ineffectiveness of systemic chemotherapy and single-agent cancer treatments have revealed the vast heterogeneity of tumors and metastases in cancer patients (*60*). In addition to the high adaptability of cancer cells to diverse environments and pressures, the innate variability of phenotypes within many solid tumors poses a seemingly insurmountable challenge for cancer treatment (*60*). Despite this, recent technological advances in the ability to tease apart and isolate cells with distinct phenotypic criteria has led to a more robust understanding of the phenotypic composition of heterogeneous solid tumors (*61*).

Phenotypic heterogeneity is a direct consequence of the abnormal proliferative nature of cancer cells, which results in genomic instability and irreparable DNA damage (*62, 63*). In healthy cells, cell division yields a 0.00001% failure rate for complete DNA replication, largely due to inherent corrective mechanisms within DNA polymerase, but also due to post-replication DNA repair mechanisms including non-homologous end joining (NHEJ) and homology-directed repair (HDR) (*64, 65*). In most healthy cells, cell division checkpoints actively pause cell division if single-strand or double-strand breaks are detected (*65*). However, cancer cells that acquire loss-of-function mutations to these checkpoint proteins or the transcription factors that govern the expression of these checkpoint proteins—such as p53—lose the ability to sense the presence of this DNA damage, resulting in premature cell division and DNA replication (*66*). Additionally, loss-of-function mutations to crucial proteins within the NHEJ or HDR mechanisms—such as BRCA1/2—also increase the incidence of somatic frameshift mutations and lower genomic fidelity during replication (*65, 67*). This decreased genomic fidelity coupled with elevated growth stimuli results in clusters of cells with high mutational burden, which

translates to the formation of a phenotypically heterogeneous tumor with multiple distinct subpopulations (*60*).

In addition to genomic diversity induced by genomic instability, there has been a growing appreciation for the epigenetic basis for phenotypic heterogeneity. During DNA replication, healthy cells also replicate DNA methylation and histone acetylation patterns with very high fidelity due to the prevalence and efficiency of writer, reader, and eraser proteins (*68*). However, abnormal regulation of the cell cycle or loss-of-function mutations to these epigenetic regulators can result in incomplete and inefficient replication of epigenetic patterns, resulting in widespread epigenetic variance (*69*). Interestingly, in some cancer subtypes, the contribution of epigenetic alterations to intratumoral heterogeneity was shown to mirror that as of genomic alterations, revealing the need to more comprehensively understand the epigenetic basis for phenotypic heterogeneity (*69, 70*).

1.2.2. Phenotypically-distinct subpopulations

A direct consequence of intratumoral heterogeneity is the emergence of phenotypically-distinct subpopulations of cells (*60*). Tumors comprised of phenotypically-distinct subpopulations boast a survival advantage over phenotypically homogeneous tumors, as different subpopulations will have different sensitivities to drug treatments and other selective pressures imposed during the process of metastasis (*71*). In non-small cell lung cancer, rare drug-resistant subpopulations were detected in multiple drug-sensitive cell lines, rendering drug treatment of these cell lines ineffective due to the prevalence of these resistant cell subpopulations (*72*). Interestingly, HDAC inhibitors and histone demethylase knockdown reduced the emergence of

these drug-resistant subpopulations, supporting an epigenetic basis for phenotypic heterogeneity within these cell lines (*72*). Similar drug-resistant subpopulations were found in metastatic breast cancer cell lines, and these drug-resistant subpopulations were found to be transcriptionally distinct to drug-sensitive subpopulations through single-cell RNA sequencing experiments (*73*).

In addition to drug resistance, subpopulations with distinct invasive properties have also been characterized in multiple cancer subtypes (*27, 30, 74*). In particular, there has been a growing interest in leader and follower subpopulations present within collectively-invading cancer cell lines (*27, 28, 29*). When isolated and purified, leader cells in non-small cell lung adenocarcinoma are highly motile and spindle-like in morphology, mirroring mesenchymal cells (*27*). Leader cells depend on filopodia for cell movement and exhibit high expression of myosin-X in their filopodia to regulate fibronectin micropatterning during cell invasion (*28*). In 3-D Matrigel matrices, leaders invade in robust chains of interconnected cells, while follower cells are significantly less motile and invade using sheet-like invasion in 3-D (*27*). Despite this decreased motility, follower cells are significantly more proliferative and maintain lower mutational burden than leader cells (*27*). Leader and follower cells also have contrasting metabolic dependencies, with leader cells predominantly using oxidative phosphorylation to convert glucose into ATP, while follower cells depend on glycolysis (*29*). Interestingly, these phenotypes are highly persistent within these subpopulations, suggesting that these cells are not in transitionally labile cell states.

In metastatic breast cancer, the existence of similarly phenotypically robust subpopulations that predominantly invade collectively or as single cells has been well documented (*74, 75, 76*). Tissue sections of breast cancer tissue both in mice and human biopsies have consistently revealed the presence of both collective chains and single cells at the invasive

edge of tumors, suggesting that cells exhibiting these phenotypes emerge together during cell invasion (*75*). Tissue fragmentation experiments using breast cancer organoids from genetically-engineered mouse models have also revealed that cells with different methods of dissemination can be isolated *in vivo* and exhibit high phenotypic persistence when purified, cultured, and re-introduced into mice (*76*). The phenotypic persistence of cell subpopulations that invade collectively or as single cells beyond primary tumor invasion is also highlighted in circulating tumor cell (CTC) quantification experiments that have shown consistent ratios of both clustered CTCs and single cell CTCs in both breast and prostate cancer blood samples (*32*). In all, these preclinical studies highlight the prevalence of invasive heterogeneity in metastatic cancers and the growing understanding of the subpopulations that these heterogeneous tumors consist of.

1.2.3. Cooperation between cancer subpopulations

Recent advances in cancer subpopulation studies have revealed that phenotypically-distinct subpopulations not only co-exist within heterogeneous primary tumors, but also have capabilities to interact and communicate (*27, 30*). Interestingly, some of these interactions between subpopulations have been shown to promote the survival and invasion of the whole tumor, further highlighting the intrinsic advantage of intratumoral heterogeneity to tumor growth and metastasis (*27, 30, 33*). In particular, subpopulation interactions in cancer have been found to mirror ecological interactions widespread in nature.

Despite the inherently competitive nature of survival, cooperation is a common behavior that is crucial to balanced and flourishing ecosystems (*77, 78*). In ecological terms, “cooperation” is defined as two or more organisms benefiting in a shared interaction with a

common goal or purpose (*79*). Many insects with societal structures such as bees and ants display highly cooperative behaviors to survive and grow beyond their available resources (*80, 81*). Notably, these organisms display stringent divisions of labor, each with designated roles that contribute to the survival and growth of the whole (*79, 81*). Many animals also cooperate to ward off predators and build long-term social bonds (*79*). Notably, vampire bats have been shown to cooperate with non-kin vampire bats by sharing blood to expand their network of possible donors over time (*82*). Additionally, behaviors such as alloparental care and punishment of selfish behaviors also demonstrate the prevalence of cooperation within the animal kingdom (*83, 84*). At the cellular level, cells within the healthy human body also cooperate to maintain structural integrity within epithelial tissues and to mount cohesive and robust immune responses against non-self entities (*85*). Classically, cancer cells have been considered to be "defectors" or "cheaters" among cooperative healthy cells due to their uncontrolled consumption of resources and rampant disregard for spatial restrictions (*86*). A growing understanding of intratumoral phenotypic heterogeneity, however, has revealed the prevalence of cooperation between cancer cell subpopulations (*27, 30, 87*). In melanoma cells, distinct "proliferative" and "invasive" subpopulations were shown to cooperate in heterotypic cell clusters, with "proliferative" cells surrounding "invasive" cells for efficient metastatic seeding (*87*). Metabolic cooperation is also common in multiple cancer subtypes wherein subpopulations that depend on glycolysis for ATP production produce lactate in hypoxic conditions for nearby cells to use (*88*).

Collective invasion is also a prominent instance of subpopulation cooperation, as "leader" and "follower" cells cooperate to advance the primary tumor beyond the basement membrane and into neighboring tissues (*24, 27, 28*). Notably, follower cells in non-small cell lung adenocarcinoma rescue mitotic deficiencies within leader cells, while leader cells use VEGF

signaling to maintain directional chain-like movement by establishing focal adhesions and secreting MMPs (*27*). Functional experiments wherein leader or follower cells were ablated showed significant abrogation of collective invasion, further supporting the cooperative nature of these heterotypic interactions (*30, 89*). Additionally, leader and follower cells in breast cancer are less transcriptionally and phenotypically distinct, but still cooperate by alternating in leading collective packs to overcome energetic barriers present when penetrating dense stromal environments (*30*). As aforementioned, collective invasion precedes the formation of heterogeneous collective packs, which enable highly resilient and robust metastatic disease due to increased resistance to immune attack and high sheer forces in the bloodstream (*31, 33, 35*). These findings suggest that cooperative interactions during tumor invasion are crucial for efficient and effective metastatic processes and are in need of further elucidation to explore therapeutic strategies to disrupt these heterotypic interactions.

1.2.4. Selfish behavior in cancer

Despite the advantages of cooperative interactions in tumor metastasis, "selfish"—or non-cooperative—behavior is frequently observed in heterogeneous solid tumors in the form of detached single cells, as aforementioned (*74, 75, 76*). Despite this, selfish behavior within cancer is less studied relative to cooperation, and the incentives for cancer cells to defect from cooperative interactions are not well understood. Computational modeling of population dynamics have revealed that selfish populations can actively benefit cooperative populations when co-existing, predominantly by trailblazing resources and space prior to the growth of cooperative populations (*90*). Yet, other computational models have predicted that selfish or "cheater" subpopulations can form highly aggressive "hypertumors" on existing tumors in large

mammals, resulting in the eradication of these initial neoplastic tumors and a possible explanation for Peto's paradox, which is the absence of correlation between cancer incidence and body size within mammals (*91*). Furthermore, selfish cancer cells have also been genetically engineered and introduced into cooperating cancer cells from multiple cancer subtypes in an effort to intervene and suppress this intratumoral cooperation with mixed results (*92*). Such efforts have highlighted the potential benefit for more comprehensively understanding the evolutionary consequences of selfish behavior within heterogeneous tumors and the mechanisms by which selfish cell subpopulations interact with cooperative cell subpopulations.

1.2.5. Parasitism and commensalism

In ecology, parasitism and commensalism are two common relationships that organisms can also share aside from cooperation (or mutualism) (*93*). In ecological terms, *parasitism* is defined as one organism benefiting from a relationship, while the other is harmed (*94*). Parasitism is commonly affiliated with arthropods, nematodes and microbial organisms, ranging from protozoans or fungi that overtake hosts for growth and survival, to fleas that live in animal hair to feed on the host's blood (*95*). Viruses are also considered parasitic to both prokaryotic and eukaryotic cells due to the unilateral benefit viruses incur through rewiring of the host's cellular machinery (*95*). As such, parasitism is the cause for the majority of infectious diseases in multicellular organisms (*96*). Similarly, cancer cells are considered to be highly parasitic to the healthy tissue they originate from and are surrounded by. As aforementioned, cancer cells classically represent "selfish" cells that disrupt the equilibrium of resource production and consumption in healthy tissues (*86*). Outgrowth of a proliferative tumor can cause severe necrosis in nearby healthy cells through nutrient depletion, hypoxia, and physical compression (*97*). Such rampant cell death left untreated at the primary tumor can ultimately cause organ

failure and potentially death in some patients (*98*). Cancer cells also have shown the potential to parasitically drive the conversion of resident macrophages to tumor-associated macrophages that become transcriptionally rewired to secrete pro-angiogenic factors such as VEGF and TNFα, and immunosuppressive cytokines such as IL-10 and TGFβ (*99*). Between cancer subpopulations, however, instances of distinctly parasitic interactions between cell subpopulations beyond basal competition have yet to be discovered.

In ecological terms, *commensalism* is defined as one organism benefiting from another organism while not being harmed or benefited itself (*100*). Generally, commensal interactions are most common between bacteria and multicellular organisms, largely due to the myriad of benefits a multicellular host can provide for resident bacteria including nutrients and a surface with consistent temperature regulation (*101, 102*). Unlike parasites, however, most resident bacteria do not harm nor provide a significant benefit to the host (*100*). Within the context of cancer, commensal interactions between cancer cells and the gut microbiome have been the most prominent, particularly in gastrointestinal malignancies (*103*). *P. gingivalis* has been shown to activate NF-κB signaling in esophageal carcinoma cells to stimulate cell proliferation and motility (*104*). In gastric cancer, *H. pylori* has been shown to secrete CagA protein, which promotes genetic instability through nuclear translocation of BRCA1 and YAP (*105*). Additionally, *H. pylori* has been shown induce CpG hypermethylation and activate ras protein activation-like protein 2 (RASAL2) to promote cell proliferation (*106*). Despite these microbes being parasitic towards the healthy human body, they are commensal to cancer cells as they actively benefit cancer cells while the bacterial populations are not benefited or harmed by the cancer cells themselves. Like parasitism, however, commensal interactions between cancer subpopulations within the same heterogeneous tumor have not been observed nor characterized.

1.3 – Dissertation goals

Intratumoral phenotypic heterogeneity poses a significant hurdle for cancer treatment due to the myriad of subpopulations that arise within a single tumor with distinct phenotypic characteristics. Recent advances in tumor heterogeneity have also characterized heterotypic interactions between phenotypically-distinct subpopulations, most notably intercellular cooperation. Despite these advances, much remains undiscovered regarding the types of interactions that cancer subpopulations depend on for effective and efficient tumor invasion and metastasis.

In this dissertation, we seek to characterize the interactions between collectively-invading cells and single cells in the 4T1 mammary adenocarcinoma cell line, which mirrors human metastatic triple-negative breast cancer. In particular, we use Spatiotemporal Genomic and Cellular Analysis (SaGA) to isolate collectively-invading cells and single cells from the 4T1 cell line, which we then characterize using a multi-omic approach involving RNA sequencing, DNA methylation analysis, and mass spectrometry-based proteomics. We then integrate these datasets and identify significant over-expression of laminin-332 components within collectively-invading cells relative to single cells. Through live cell experiments, we find that laminin-332 secreted from collectively-invading cells bolsters the invasive potential of single cells by increasing cell velocity and directionality of movement. We further interrogate the mechanistic underpinnings of this interaction and find that laminin-332 binds to integrin $\alpha 6/\beta 4$ to activate Rac1 in single cells. In all, this dissertation highlights a novel commensal interaction between phenotypically heterogeneous cancer subpopulations in metastatic triple-negative breast cancer.

Chapter 2: Subpopulation commensalism promotes Rac1-dependent invasion of single cells via laminin-332

2.1 – Author's Contribution and Acknowledgment of Reproduction

Portions of this chapter were reproduced with edits from:

S. B. Yoon*, L. Chen, I. E. Robinson, T. O. Khatib, R. A. Arthur, H. Claussen, N. M. Zohbi, H. Wu, J. K. Mouw and A. I. Marcus. 2024. Subpopulation commensalism promotes Rac1-dependent invasion of single cells via laminin-332. *The Journal of cell biology*. 223(6):e202308080.

S.Y., J.K.M. and A.I.M. designed the experiments. J.K.M. and N.M.Z. performed SaGA to isolate 4T1 subpopulations. S.Y., J.K.M., I.E.R., and T.O.K. performed the experiments. S.Y., R.A.A., H.C., and L.C. contributed to the bioinformatics and statistical analysis of the transcriptomics and epigenomics data. S.Y., R.A.A., H.C., and L.C. drafted the manuscript. All authors provided input and feedback during manuscript preparation and edited the manuscript.

2.2 Abstract

Phenotypic heterogeneity poses a significant hurdle for cancer treatment but is under-characterized in the context of tumor invasion. Amidst the range of phenotypic heterogeneity across solid tumor types, collectively-invading cells and single cells have been extensively characterized as independent modes of invasion, but their intercellular interactions have rarely been explored. Here, we isolate collectively-invading cells and single cells from the heterogeneous 4T1 cell line and observe extensive transcriptional and epigenetic diversity across these subpopulations. By integrating these datasets, we identify laminin-332 as a protein complex exclusively secreted by collectively-invading cells. Live cell imaging revealed that laminin-332 derived from collectively-invading cells increased the velocity and directionality of single cells. Despite collectively-invading and single cells having similar expression of the integrin α6β4 dimer, single cells demonstrated higher Rac1 activation upon laminin-332 binding to integrin α6β4. This mechanism suggests a novel commensal relationship between collectively-invading and single cells wherein collectively-invading cells promote the invasive potential of single cells through a laminin-332/Rac1 axis.

2.3 Introduction

Tumor heterogeneity poses a significant hurdle to cancer treatment (*60, 70, 107, 108, 109*). In particular, phenotypic heterogeneity—defined as distinct morphological and behavioral characteristics of subpopulations within a group of cells—plays a crucial role in therapeutic resistance (*110*). Identifying and characterizing the subpopulations that emerge as a tumor evolves are crucial to uncovering potential vulnerabilities for multi-targeted therapy.

Within this wide range of phenotypic heterogeneity, recent studies have revealed the prominence of invasive heterogeneity across solid tumors (*27, 30, 75, 111*). Notably, human tissue sections of breast tumors show a co-existence of collectively-invading packs alongside single cells at the invasive edge (*75*). Intravital imaging of murine breast tumors corroborates these invasive modalities and demonstrates the spontaneous emergence of these distinct subpopulations upon mammary fat pad implantation (*74*). Additionally, primary organoids from a genetically engineered mouse model of triple-negative breast cancer revealed that cells that persistently invade collectively or as single cells could be separated from the same tumor (*76*). Furthermore, circulating tumor cell (CTC) analysis in breast and prostate cancer patients have identified both circulating tumor clusters and single cells (*32*), supporting the maintenance of invasive heterogeneity after initial primary tumor invasion.

As separate mechanisms of invasion, collective and single-cell invasion have been extensively characterized (*24, 26, 112, 113, 114*). Despite these observations, the interactions between invasively-distinct subpopulations require further elucidation. Collective invasion depends on the formation of an extensive network of cell-cell junctions to maintain cell-cell adherence during cell motility (*115, 116*). Collective “chains” of cells extend outward through highly motile leader cells, which drive directional movement through invadopodial protrusions in

3D and fibronectin micropatterning (*27, 28*). Collective packs of tumor cells have enhanced capabilities to intravasate into the circulation (*15*), override pro-apoptotic signaling induced by ECM detachment (*117*), and evade immune attack (*118*). Conversely, single cell invasion occurs independently of cell-cell junctions, exchanging invasive efficiency for dynamic flexibility. Single cell invasion is largely split into mesenchymal or amoeboid with the former dependent on filopodia and matrix metalloproteases to move, and the latter being independent of such protrusions and instead relying on physical cellular deformation to navigate porous extracellular matrix environments such as collagen (*24, 114*). The dynamic nature of amoeboid movement allows for cells to exhibit drastically higher velocities than collective packs whilst simultaneously being highly proliferative, enabling efficacious metastatic seeding into the lung, bones and nearby lymph nodes (*46, 119*). Despite extensive characterization of collective and single-cell motilities in cancer cells, little is known about how subpopulations that adopt these phenotypes interact to drive local cell invasion.

Recent discoveries have pointed to the predisposition for distinct subpopulations to interact to drive invasion and metastasis across multiple cancer models. “Proliferative” and “invasive” subpopulations of zebrafish melanoma cells have been shown to cooperate within metastatic clusters through TFAP2 to drive invasion (*87*). In human lung adenocarcinoma cell lines, distinct “leader” cells within invasive collective chains used VEGF signaling to bolster the invasive potential of “follower” cells, while follower cells actively secreted growth signals to support leader cell survival (*27*). Leader and follower cell dynamics have also been observed in breast cancer cells, wherein metabolically distinct leader and follower cells spatiotemporally alternate leading collective packs to overcome the energy barrier required for effective invasion through dense collagen matrices (*30*). Furthermore, ablation and isolation experiments wherein

leader or follower cells were deprived of heterotypic interactions demonstrated suppression of overall invasion in a myriad of cancer subtypes (*30, 89, 120*). Despite these advances, the underlying mechanisms governing the interactions between collectively-invading and single cell subpopulations have yet to be explored.

Here, we sought to isolate the distinct subpopulations observed in triple-negative mammary carcinoma invasion to determine how invasively heterogenous subpopulations interact. We implemented an image-guided technique developed in our laboratory to precisely isolate cells that invade as collective packs or as single cells. RNA sequencing of collectively-invading cells and single cells revealed vastly distinct transcriptional programs between these subpopulations. This prompted us to take a multi-omic approach involving RNA sequencing, methylation and proteomic analysis to identify proteins that collectively-invading cells secrete to alter single cells, and found laminin-332 components to be highly expressed and secreted in collectively-invading cells. We show that laminin-332 increases the velocity and directionality of single cells through live cell imaging and uncover an enhanced capability for singles to utilize laminin-332 through integrin a6b4 to hyperactivate Rac1. Our work sheds light on the transcriptional and behavioral heterogeneity between collectively-invading and single cells and suggests a novel commensal relationship—whereby one subpopulation benefits from another subpopulation that is not being harmed nor benefited—between these subpopulations within a highly heterogeneous triple-negative breast cancer model.

2.4 Methods

Cell culture conditions

4T1 cells [American Type Culture Collection (ATCC); gift from Harold Moses (Vanderbilt University)] were cultured in DMEM media treated with penicillin-streptomycin (100 U mL^{-1}) and supplemented with 10% fetal bovine serum (FBS) and maintained at 37°C and 5% CO_2. SUM159 cells [gift from Paula Vertino (University of Rochester)] were cultured in DMEM/F12 media supplemented with 5% FBS, 5 μg/mL insulin, 1 μg/mL hydrocortisone and treated with penicillin-streptomycin (100 U mL^{-1}) and maintained at 37°C and 5% CO_2. HCC38 cells [gift from Jennifer Spangle (Emory University)] were cultured in RPMI media treated with penicillin-streptomycin (100 U mL^{-1}) and supplemented with 10% fetal bovine serum (FBS) and maintained at 37°C and 5% CO_2. Leader, follower and singles subpopulations were isolated from 4T1 cells transfected with H2B-Dendra2 using SaGA, as previously described (*27, 61*). Briefly, 4T1 cells were transfected with nucleus-targeting H2B-Dendra2, a photoconvertible fluorescent protein that facilitates cell visualization during imaging. Prior to photoconversion, all cells emit green fluorescence (maximum excitation, 490 nm; maximum emission, 507 nm) and after excitation with a 405 nm laser, H2B-Dendra2 within selected cells photoconverts to emit red fluorescence (maximum excitation, 553 nm; maximum emission, 573 nm). While cells were invading in 3-D collagen type I, individual leader, follower and single cells were photoconverted separately without fluorescence conversion occurring in nearby cells. After photoconversion, cells were extracted from the collagen type I matrix and sorted using flow cytometry. All isolated subpopulations were authenticated as 4T1 cells via STR analysis by IDEXX Laboratories Inc. (Columbia, MO) and as such were determined to be free of contamination from another cell line. All cell lines were routinely tested for mycoplasma contamination using a commercially

available kit (MycoAlert Mycoplasma Detection Kit; Lonza) according to the manufacturer's instructions.

Plasmids, transfections, and transductions

4T1 cells were transfected using Lipofectamine 3000 (Thermo Fisher Scientific, L3000001), per the manufacturer's instructions, or transduced using lentiviral supernatant produced by 293T cells (*121*) with selection based on H2B-Dendra2 expression via flow cytometry. The pLenti.CAG.H2B-Dendra2.W was a gift from Rusty Lansford (Addgene plasmid #51005; http://n2t.net/addgene:51005; RRID:Addgene_51005). Sleeping Beauty transfections were performed using a 2:1 ratio of transposon to transposase ratio. The pSBbi-Pur-mCherry transposon vector and pCMV(CAT)T7-SB100 transposase vector were gifts from Eric Kowarz (Addgene plasmid # 60523; http://n2t.net/addgene:60523; RRID:Addgene_60523). CRISPR-Cas9 knockout of *mLama3* on leaders and clonal isolation of knockout cells was performed by Synthego (Redwood City, CA) (*mLama3* gRNA: CUGCGGGGAGCGGGACCCAG). piggyBac transfections were performed using a 1:1 molar ratio of transposon vector to transposase mRNA ratio. *mItga6* shRNA knockdown and scrambled vectors (shRNA target sequences: CGGAAATCCTTTCAAGAGAAA, CGAGAAGGAAATCAAGACAAA) and were designed and purchased from VectorBuilder (Chicago, IL).

Reagents and antibodies

E-cadherin (CDH1) (Cell Signaling, 24E10) was used at 1:10,000 for immunoblotting and 1:500 for immunostaining. Laminin-5 (Abcam, ab14509) was used at 1:200 for immunostaining for

1:1000 for immunoblotting and experiments requiring inhibition of laminin-332 interactions. Integrin alpha 6 (Abcam, ab181551) was used at 1:1,000. Integrin alpha 6-APC (R&D Systems, FAB13501A) was used for flow cytometry. Integrin beta 4 (Abcam, ab236251) was used at 1:1,000. Actin (Sigma-Aldrich, A2066) was used at 1:10,000. Peroxidase AffiniPure Goat Anti-Rabbit IgG (H+L) (Jackson ImmunoResearch, 111-035-144) was used at 1:10,000. For laminin-332 experiments, human Biolaminin-332 (BioLamina, LN332-0202) was adsorbed per manufacturer's instructions. Manganese (II) chlorine solution (Sigma-Aldrich, M1787) was used at 1 mM to activate integrins.

RNA-seq

RNA-seq was performed in triplicate on 4T1 leader, follower and single cells. Cells were grown to 70% confluency and RNA was extracted using an RNeasy Mini Kit (Qiagen, 74104). RNA quality control and quantification were performed by the Emory Integrated Genomics Core using a Bioanalyzer and Nanodrop. RNA-seq library preparation was performed at Novogene (Durham, NC) utilizing the NEBNext Ultra RNA Library Prep Kit for Illumina (New England Biolabs, E7530) by following the manufacturer's recommendations. Sequencing libraries were validated on the Agilent 2100 Bioanalyzer System (Agilent Technologies) and quantified using Qubit 2.0 Fluorometer (Invitrogen) as well as by quantitative PCR (Applied Biosystems). The libraries were sequenced to 50M reads per sample on an Illumina sequencer using a 2x150 Paired End (PE) configuration. Raw sequence data (.bcl files) was converted into fastq.gz files and de-multiplexed using Illumina's bcl2fastq software. Compressed, raw sequence data in fastq.gz format were trimmed using Trimmomatic v0.36 (*122*) to remove Illumina adapter contamination using parameters ILLUMINACLIP:20:10:8:TRUE in paired-end mode, and

checked for quality control using FastQC v0.11.4 and MultiQC v1.12 (*123*) to generate complete QC reports in HTML format. Trimmed data were also analyzed in FastQC to ensure removal of adapter content and then were aligned to the mm10 mouse reference genome using STAR aligner v2.5.2 (*124*) with default parameters. HTseq-count v0.13.5 (*125*) was used via gene-id method to assign counts per gene with the parameters "htseq-count -f bam -m union -r pos -i gene_id -a 10 -s no". The resulting counts tables per sample were merged into an overall counts matrix and analyzed downstream in DESeq2.

DESeq2 was used to determine differentially expressed genes between two experimental groups (*126*). Raw gene expression counts were used as DESeq2 internally corrects for library size. The expression count table was assumed to follow a negative binomial distribution and the Wald Test was implemented for differential gene expression testing. Raw p-values were transformed using the Benjamini-Hochberg correction and a corrected p-value of less than 0.05 was considered for statistical significance (*127*). Heatmaps were generated using the R package pheatmap following the application of a variance stabilizing transformation (*128*). Volcano plots were generated using the R package EnhancedVolcano.

DNA methylation microarray

DNA methylation status was assessed in triplicate on 4T1 leader and single cells. Cells were grown to 70% confluency, trypsinized and then homogenized using QIAshredder (Qiagen, 79654). DNA was isolated using the QIAamp DNA Mini Kit (Qiagen, 51304). DNA quality control was performed through the Quant-iT Broad-Range dsDNA assay kit (Invitrogen,

Q33130) and agarose gel by the Emory Integrated Genomics Core. AKESOgen (Peachtree Corners, GA) performed an upfront quantification assay using the Quant-iT PicoGreen dsDNA assay kit (Invitrogen, P7589) to confirm DNA concentration and volume. Bisulfite conversion was performed on the DNA, and the DNA was applied to the Infinium Mouse Methylation BeadChip (Illumina, 20041558) and reagents. Data from each sample was first pre-processed by R package "sesame" (*129*), which includes masking sub-optimal probes (e.g., detection p-value > 0.01, on X and Y chromosomes, non-CpG probes, SNP-related probes, and repetitive element), background subtraction, and type-1 probe dye bias. The bias of type-2 probe values was corrected by method "BMIQ" implemented in R package "wateRmelon" (*130*). Batch effect was corrected by "combat" method in R package "ChAMP" (*131*) and between-array normalization was completed by R package "qsmooth" (*132*). Differentially methylated positions (DMPs) between group leaders and group singles were detected by function "dmpFinder" implemented in R package "minfi" (*133*) with criteria absolute beta value difference greater than 0.2 and q-value smaller than 0.05. Differentially methylated regions (DMRs) were identified with function "combp" implemented in R package "ENmix" (*134*) with the following criteria: absolute difference of average betas in a region greater than 0.2, probe number greater than 1, sidak correction p-value smaller than 0.1 and minimum region size greater than 50 bp. Gene promoter information was derived from the ENCODE Project.

LC-MS/MS

Proteomic analysis was performed on the conditioned media of adherent cells in 2-D plastic. Cells were grown to 50% confluency in complete media, then washed with 1× PBS before replacing with a serum-free defined media supplemented with 1× insulin-transferrin-selenium-

ethanolamine, 0.5 µg/mL hydrocortisone, 1 ng/mL cholera toxin, 50 nM *O*-phosphorylethanolamine, 5 nM triiodothyronine and 10 ng/mL human EGF. Conditioned media was collected over 48 h, centrifuged at top speed using Vivaspin 20, 3 kDa MWCO polyethersulfone filters (Cytiva, 28-9323-58) at 4 C to extract secreted proteins, then flash frozen. Protein extracts were processed through the Emory Integrated Proteomics Core as previously described (*135*). Briefly, samples were normalized with 50 mM NH_4HCO_3, then treated with 5 mM dithiothreitol (DTT) at RT for 30 minutes, followed by 10 mM iodoacetimide (IAA) at RT for 30 minutes in the dark. Protein digestion was performed with 4 µg of lysyl endopeptidase (Fujifilm Wako Chemicals, 101974-094) at RT overnight and proteins were further digested overnight with 4 µg trypsin. Resulting peptides were desalted with an HLB column (Waters, 186002034) and were vacuum dried.

Data acquisition by LC-MS/MS was adapted from a published procedure (*136*). Digested peptides were resuspended in 0.1% trifluoroacetic acid and separated on a Water's Charged Surface Hybrid (CSH) column (150 µm internal diameter (ID) x 15 cm; particle size: 1.7 µm). An EVOSEP liquid chromatography system was used to run the samples using the preset gradient (88 min). Samples were then monitored on a Q-Exactive Plus Hybrid Quadrupole-Orbitrap Mass Spectrometer (ThermoFisher Scientific). The mass spectrometer cycle was programmed to collect one full MS scan followed by 20 data dependent MS/MS scans and MS scans (400-1600 m/z range, 3 x 106 AGC target, 100 ms maximum ion time) were collected at a resolution of 70,000 at m/z 200 in profile mode. The HCD MS/MS spectra (1.6 m/z isolation width, 28% collision energy, 1 x 105 AGC target, 100 ms maximum ion time) were acquired at a resolution of 17,500 at m/z 200. Dynamic exclusion was set to exclude previously sequenced

precursor ions for 30 seconds. Precursor ions with +1, and +7, +8 or higher charge states were excluded from sequencing.

Label-free quantification analysis was adapted from a published procedure (*136*). Andromeda was used to search the spectra, which where subsequently integrated into MaxQuant, against the 2020 Uniprot mouse database (91,439 target sequences). Methionine oxidation (+15.9949 Da), asparagine and glutamine deamidation (+0.9840 Da), and protein N-terminal acetylation (+42.0106 Da) were variable modifications (up to 5 allowed per peptide); cysteine was assigned as a fixed carbamidomethyl modification (+57.0215 Da). Only fully tryptic peptides were considered with up to 2 missed cleavages in the database search. A precursor mass tolerance of ±20 ppm was applied prior to mass accuracy calibration and ±4.5 ppm after internal MaxQuant calibration. The following additional search settings were also included: a maximum peptide mass of 6,000 Da, a minimum peptide length of 6 residues, 0.05 Da tolerance for orbitrap, and 0.6 Da tolerance for ion trap MS/MS scans. The false discovery rate (FDR) for peptide spectral matches, proteins, and site decoy fraction were all set to 1%. The following quantification settings were applied: re-quantify with a second peak finding attempt after protein identification has completed; match MS1 peaks between runs; a 0.7 min retention time match window was used after an alignment function was found with a 20-minute RT search space. Protein quantification was performed using summed peptide intensities given by MaxQuant. The quantitation method only considered razor plus unique peptides for protein level quantitation.

3D invasion assays and spheroid microscopy

Spheroids were generated, as previously described (*137*). Cells were seeded in round bottom 96-well plates at a density of 1,000 cells per well and centrifuged at 1500 RPM for 5 minutes. After incubating the plate at 37°C and 5% CO_2 for 72 h, spheroids were embedded in 3 mg/mL rat-tail collagen type I (Corning, 354249) and seeded unto glass-bottom culture dishes (MatTek, P35G). The collagen matrix was allowed to polymerize at 37°C and 5% CO_2 for 30 minutes prior to media supplementation.

Images were taken using an Olympus CKX41 microscope with an Infinity 1-3C camera [×4 air, 0.13 numerical aperture (NA), UPlanFL N] at RT using Infinity image acquisition software. For spheroids with mixed subpopulations, cells were seeded together in round-bottom 96-well plates at a 1:1 ratio with 1,000 total cells per spheroid. Images of spheroids that required fluorescent imaging were taken with the Leica TCS SP8 inverted confocal microscope (×10) using 1-mm stack intervals, line scanning (488-nm argon, 561-nm diode-pumped solid-state), 4× line averaging, and both HyD and PMT detectors. Images were acquired at RT using Leica image acquisition software. Leica software was also used post-acquisition to perform maximum projections on multi-stack acquisitions and to export processed images.

Immunoblotting and immunostaining

For immunoblotting, whole cell lysate protein expression was assessed by western blotting. Briefly, adherent cells were rinsed with 1× phosphate-buffered saline (PBS) with Ca^{2+} and Mg^{2+} and lysed with RIPA buffer [50 mM Tris (pH 7.8), 2 mM EDTA, 150 mM NaCl, 1% Triton X-100, 5% SDS, 5% sodium deoxycholate] supplemented with Halt Protease and Phosphatase

Inhibitor Cocktail (Thermo Fisher Scientific, 78429). Lysates were then sonicated briefly to shear the DNA. Protein quantification was performed using a bicinchoninic acid (BSA) protein assay kit (Thermo Fisher Scientific, 23225) before SDS–polyacrylamide gel electrophoresis. After electrophoresis, proteins were transferred from the gel to a nitrocellulose membrane for 2 h at 300 mA. The membrane was then blocked using 5% milk diluted in TBS-T for 1 h at RT prior to incubating with the primary antibody overnight at 4°C while rocking. After several washes with TBS-T, the membrane was incubated with the secondary antibody at RT for 50 min. Membranes were treated with horseradish peroxidase and developed via film or digital imaging.

For immunostaining (*138*), cells in 2D or spheroids embedded in rat-tail collagen type I were rinsed with 1× PBS with Ca^{2+} and Mg^{2+} and then immediately fixed with freshly prepared 4% paraformaldehyde diluted in 1× PBS with Ca^{2+} and Mg^{2+} for 20 min at room temperature. Spheroids were then rinsed with 100 mM glycine diluted in immunofluorescence buffer (130 mM NaCl, 7 mM Na_2HPO_4, 3.5 mM NaH_2PO_4, 0.2% Triton X-100, 0.05% Tween-20) prior to blocking with immunofluorescence buffer supplemented with 10% normal goat serum for 1 h at RT while rocking. Spheroids were then incubated with primary antibody overnight at 4°C while rocking. Spheroids were then washed with immunofluorescence buffer prior to secondary antibody incubation at RT for 50 minutes. After staining, cells in 2D or 3D spheroids were imaged using the Leica TCS SP8 inverted confocal microscope (×10) using 1-mm stack intervals, line scanning (488-nm argon, 561-nm diode-pumped solid-state), 4× line averaging, and both HyD and PMT detectors.

Flow cytometry

Relative expression of cell surface proteins and detection of cell apoptosis was measured through flow cytometry. For measuring the expression of cell surface proteins, adherent cells were seeded in 10 cm culture plates and grown to 80% confluency prior to dissociation with 1 mM EDTA diluted in 1X PBS. After dissociation, suspended cells were centrifuged into a pellet, washed, and stained with a fluorophore-conjugated antibody diluted in flow buffer (1 mM EDTA, 25 mM HEPES, 1% dialyzed FBS diluted in 1X PBS) for 30 minutes at 4 C in the dark while agitated. Cells were then washed with flow buffer prior to resuspension for analysis using a BD FACSymphony A3. For detection of cell apoptosis, the PE Annexin V Apoptosis Detection Kit I (BD Pharmigen, 559763) was used, per manufacturer's instructions. All data was further analyzed using FlowJo.

Live-cell imaging

Spheroids were embedded in rat-tail collagen type I and plated into cell culture plates with optical glass bottoms as previously described (*27*). Spheroids were then imaged using the Leica TCS SP8 inverted confocal microscope (×10) with a live-cell chamber (37°C and 5% CO_2) using 1-mm stack intervals, line scanning using a resonant galvanometric tandem scanner (8 kHz; 488-nm argon, 561-nm diode-pumped solid-state), 4× line averaging, and both HyD and PMT detectors. For conditioned media experiments where no fluorescence was required for image acquisition, images were acquired every 20 minutes for 24 hours. For mixed spheroid experiments, images were acquired every 20 minutes for 48 hours. Leica image acquisition

software was used to acquire images and to perform maximum projections on multi-stack images post-acquisition.

Image analysis

For image sequences of 3D spheroids, each 3D image (*x*, *y* and *z*) was flattened to 2D maximum projections (*x* and *y*). Relative velocity and track length of individual cells in 3D spheroids were measured using the MTrackJ plug-in in ImageJ (*139*). Tracks were drawn by manually selecting a random cell and following the cell's movement at every time point in the image sequence. 5 tracks were drawn per spheroid for 3 separate spheroids for each condition. Circularity of individual cells was measured at the end of each image sequence by manually outlining the cell border using ImageJ. 5 random cells were chosen from a randomized region for 3 separate spheroids for each condition.

Rac1 G-LISA

Rac1 activity was measured using the colorimetric Rac1 G-LISA Activation Assay Kit (Cytoskeleton, BK128) per manufacturer's instructions. Cells were grown to 70% confluency with complete media and then serum-starved overnight with serum-free DMEM media. For experiments wherein cells were treated with conditioned media derived from other cells, cells were pre-treated with 1 mM Mn^{2+} diluted in serum-free DMEM for 10 minutes to activate integrins. Proteins from conditioned media were extracted by centrifugation using Vivaspin 20, 3 kDa MWCO polyethersulfone filters (Cytiva, 28-9323-58) and protein concentration was quantified using a BSA protein assay kit (Thermo Fisher Scientific, 23225). Protein

concentrations were normalized for each experiment and diluted in serum-free DMEM supplemented with 1 mM Mn^{2+} before stimulating serum-starved cells.

Statistical analysis

Statistical analyses were performed using GraphPad Prism. For all experiments with a single variable and data points acquired from two independent samples, unpaired student T-tests were performed to evaluate significance. For all experiments with a single variable and data points acquired from three independent samples, one-way ANOVA tests with multiple comparisons were performed. For all experiments with two variables, two-way ANOVA tests with multiple comparisons were performed. For all ANOVA tests with multiple comparisons, a Tukey correction was applied. For all parametric tests, data distribution was assumed to be normal but this was not formally tested. All bar graph data show the mean, with error bars indicating SEM. For violin plots, thicker segmented lines indicate the mean, while the thinner segmented dots indicate the interquartile range. The figure legends indicate the number of biological replicates (*n*) for each experiment and all significance denotations.

2.5 Results

Collectively-invading cells and single cells can be isolated as distinct invasive subpopulations

We used SaGA to isolate collectively-invading cells and single cells from invading 4T1 spheroids (*61*). Collectively-invading cells were identified and isolated as cells invading while maintaining cell-cell junctions. Within a chain, *leaders* were isolated as the tip-most cell of a chain. Cells posterior to the leader and separated by 2-3 intermediate cells were isolated as *followers* (*29*). Conversely, *singles* were identified and isolated as individual cells that were not visually attached to other cells and were separated from the parental spheroid by multiple cell body lengths (Figure 1A, 1B). After sorting, isolated and purified leaders, followers, and singles were maintained separately and their phenotypes were assessed in 2-D and 3-D culture. In 2-D culture, leaders and followers continued to invade collectively and maintained a high density of E-cadherin positive cell-cell junctions (Figure 1C-E, Supplementary Figure 1A). Singles, in contrast, resembled a rounded amoeboid phenotype with little to no E-cadherin positive cell-cell junctions present between cells (Figure 1C-E, Supplementary Figure 1A). We did not observe expression of other cadherin junction proteins such as N-cadherin or P-cadherin within any of our subpopulations (Figure 1D). When embedded in a 3-D type I collagen microenvironment, SaGA-isolated leaders and followers exhibited collective movement, wherein cells would aggregate in chains to penetrate the surrounding stroma in a linear, unidirectional manner while singles invaded exclusively as detached, individual cells (Figure 1C). Surprisingly, these morphological and invasive phenotypes were retained over more than 40 passages, suggesting that leaders, followers, and singles are not merely cells existing in transient phases, but stable subpopulations with distinct programs that define their cellular behavior. Importantly, we have

also observed invasive heterogeneity in the human SUM159 and HCC38 triple negative breast cancer cell lines. Similar to the 4T1 parental cell line, we observe both cell-cell adherent collectively-invading cells and detached single cells within the same spheroid (Supplementary Figure 1B). Taken together, these data support the presence of phenotypic heterogeneity across multiple cancer models, consistent with other published reports (*74, 75, 76*)

Collectively-invading cells and singles are transcriptionally and epigenetically distinct

To investigate potential underlying drivers governing the invasive phenotypes of the leader, follower, and single subpopulations, we performed bulk RNA sequencing on our purified subpopulations (Figure 2A). Principal component analysis revealed that singles have a distinct transcriptional profile when compared to leaders and followers (Figure 2B). Leaders and singles exhibited 1412 differentially-expressed genes (DEGs; $|\log_2$ fold-change$| > 2$, adjusted p-value < 0.05), while followers and singles exhibited 991 DEGs (Figure 2D); importantly, both pair-wise comparisons included E-cadherin (*Cdh1*) as a highly expressed gene transcript in leaders and followers relative to singles (Figure 2C). In addition to *Cdh1*, leaders and followers also overexpressed *Tacstd2*, *Krt14*, *Esrp1, Cldn4,* and *Lama3*, all of which exhibited greater than a 7.0 $\log_2$-fold change when compared to singles (Figure 2E). When Gene Ontology was performed, leaders and followers showed enrichment in multiple gene sets including *substrate-dependent cell migration* (GO:0006695), *cell-cell adhesion* (GO:0098609) and *tight junction assembly* (GO:0120192) when compared to single cells. Conversely, single cells overexpressed *Loxl3*, *Prex1*, and *Il17rd* when compared to collectively-invading cells (Figure 2C), and showed enrichment in *Collagen biosynthesis and modifying enzymes* (R-HSA-1650814), *RAC1 GTPase*

cycle (R-HSA-9013149), and *Signaling by Receptor Tyrosine Kinases* (R-HSA-9006934) gene sets.

Interestingly, leaders and followers exhibited only 416 DEGs, suggesting that leaders and followers within the 4T1 cell line are transcriptionally similar subpopulations (Figure 2D). This result is consistent with evidence presented previously (*30*) detailing the fluidity of leader and follower phenotypes in breast cancer models. Due to this phenotypic and transcriptional fluidity, we proceeded to represent collectively-invading cells with the leader subpopulation.

To determine whether the transcriptomic differences between leaders and singles have an underlying epigenetic basis, we performed methylation analysis on leaders and singles. Like the RNA sequencing analysis, we observed stark differences in the methylation patterns of CpG sites across the epigenome of leaders and singles (Figure 2F). Leaders and singles exhibited 1714 differentially-methylated regions (DMR; beta difference <-0.2 and >0.2), with singles exhibiting hypermethylation in 95.9% of its DMRs (Figure 2G). Among the hypermethylated CpG sites in singles, CpG sites across the gene bodies of *Cdh1*, *Tacstd2, Krt14, Esrp1, Cldn4* and *Lama3* were significantly hypermethylated in singles with a mean beta score of 0.17, while being hypomethylated in leaders at a mean beta score of 0.75 (Figure 2H). Notably, *Cdh1, Tacstd2, Cldn4* and *Lama3* each had at least one differentially methylated position (DMP) within the promoter region. These data suggest that the methylation patterns that differentiate leaders and singles parallel the transcriptomic differences found between these subpopulations in the RNA sequencing analysis. These similarities support a methylation-driven transcriptional heterogeneity of invasively-distinct subpopulations, with singles notably exhibiting down-regulation of key genes due to inherent hypermethylation of CpG sites across its cell genome. Taken together, these analyses show that collectively-invading cells and single cells have distinct

transcriptional and epigenetic programs that likely underlie their respective morphological and behavioral phenotypes.

Multi-omic analyses reveal overexpression of laminin-332 in collectively-invading cells

To identify gene transcripts that are both transcriptionally upregulated and hypomethylated at the promoter region of collectively-invading cells relative to singles, we integrated RNA sequencing and methylation array data from leaders and singles. Among the 9 most over-expressed and hypomethylated gene transcripts in leaders, we identified two components of the laminin-332 complex, laminin alpha chain-3 (*Lama3*) and laminin gamma chain-2 (*Lamc2*) (Figure 3A). Compared to singles, leaders expressed 673-fold higher mRNA counts of *Lama3* and 95-fold higher mRNA counts of *Lamc2* (Figure 3B,C), while also exhibiting a mean beta difference of 0.23 and 0.45 in the promoter regions of the *Lama3* and *Lamc2* genes, respectively (Figure 3D). Additionally, the third component of the laminin-332 complex, laminin beta chain-3 (*Lamb3*) had 144-fold higher mRNA counts in leaders (Figure 3B) while also exhibiting a mean beta difference of 0.30 in the gene promoter (Figure 3C). To confirm that this enrichment in laminin subunits in leaders was not due to an overexpression of all laminins, we measured the relative expression of each laminin detected within our RNA sequencing dataset. Surprisingly, only 5 out of the 11 laminin subunits detected within the array were overexpressed in leaders, and the three most overexpressed subunits were *Lama3*, *Lamb3* and *Lamc2*, confirming the specific upregulation of the laminin-332 complex within leaders (Supplementary Figure 2).

To determine if laminin-332 protein was preferentially secreted by leaders, we performed an unbiased proteomic analysis using mass spectrometry on purified protein extracts from conditioned media of leaders and singles. Among the 17 most differentially secreted proteins present in leader conditioned media, laminin subunits α3 (Lama3), β3 (Lamb3), and γ2 (Lamc2) were all highly abundant exclusively in leaders (Figure 3E). In contrast, no protein was detected for Lama3, Lamb3 and Lamc2 in singles, corroborating the binary nature of laminin-332 secretion by leaders (Figure 3F). Western blot analysis also revealed that laminin-332 was drastically overabundant in leaders conditioned media when compared to singles (Figure 3G). 2-D and 3-D immunofluorescence staining using a laminin-332 antibody revealed higher expression of laminin-332 in leader spheroids than single spheroids (Figure 3H). Together, these data demonstrate that components of the laminin-332 complex are not only transcriptionally and epigenetically overrepresented in collectively-invading cells, but also exclusively and abundantly secreted as proteins by collectively-invading cells.

Laminin-332 promotes the 3-D invasion of singles

The secretion of laminin-332 complex exclusively by collectively-invading cells led us to hypothesize that collectively-invading cells could influence the invasive potential of single cells via laminin-332. To test this, we first observed the behavior of singles when treated with laminin-332-expressing leader conditioned media (CM) compared to laminin-332-low single CM in a 3-D spheroid model. Within a 24-hour time period, singles treated with leader CM exhibited a significantly higher velocity and track length than singles treated with single CM (Figure 4A). Additionally, singles treated with leader CM displayed a higher potential for directional movement through decreased cellular circularity and a higher meandering index (defined as

displacement divided by distance) than singles treated with single CM (Figure 4A, Supplementary Figure 3A). To confirm the specific role of laminin-332 in the elevated invasive potential of singles, we treated singles with conditioned media from leaders with a CRISPR/Cas9 knockout of the *Lama3* gene. Western blot analysis of the conditioned media of the knockout cells confirmed that *Lama3* knockout was sufficient for reducing laminin-332 complex assembly and did not hinder the viability or invasive behavior of leaders (Figure 4B, Supplementary Figure 3D). Singles treated with conditioned media from two distinct clones of *Lama3* knockout leaders (clones C1 and D4) showed considerable repression of cell movement, velocity, and directionality when compared to singles treated with conditioned media from leaders with only the Cas9 endonuclease transfected (*Lama3* WT cells) (Figure 4C, Supplementary Figure 3B).

We further validated the role of laminin-332 in stimulating the invasive potential of single cells by co-culturing *Lama3*-expressing or *Lama3*-null leaders with singles within a mixed 3-D spheroid. Singles were transfected with mCherry-Red and mixed with leaders with wildtype *Lama3* or *Lama3* knockout at a 1:1 ratio within a single spheroid, and allowed to invade in collagen type I over 48 hours (Figure 4D). Singles that were mixed with leaders with *Lama3* knockout invaded significantly less and with less directionality than leaders with *Lama3* wildtype (Figure 4D, Supplementary Figure 3C), supporting a model whereby local laminin-332 secretion by collectively-invading cells promotes directional invasion in single cells within a heterogeneous tumor environment.

Singles hyperactivate Rac1 upon laminin-332 binding

The effect of laminin-332 on the invasive potential of singles led us to investigate the underlying molecular mechanism by which cell movement was being stimulated within singles. We sought to test whether singles over-express receptors that specifically bind to laminin-332. Canonically, laminin-332 binds to the integrin pairs α6/β4 and α3/β1, each resulting in the downstream activation of distinct small GTPase signaling cascades, Rac1 and Rho, respectively (*140*). RNA sequencing analysis of integrin expression between leaders and singles revealed that singles only showed significant transcriptional over-expression of integrins α6 (*Itga6*) and β4 (*Itgb4*) relative to leaders, while integrins α3 and β1 were overexpressed in leaders relative to singles (Figure 5A, 5B). Interestingly, Western blot analysis on whole cell lysates of leaders and singles revealed no notable difference in total protein expression of integrins α6 and β4 in singles relative to leaders (Figure 5C). Furthermore, flow cytometric detection of cell surface integrin α6 expression also showed no significant differences in protein abundance between leaders and singles (Supplementary Figure 4A). Thus, we hypothesized that singles exclusively activate Rac1 via the integrin α6/β4 receptor, despite leaders also expressing the heterodimer.

To test this, we first evaluated the response of leaders and singles to Rac1 stimulation via EGF treatment. Interestingly, EGF exclusively led to Rac1 activation in singles, while in leaders we observed a gradual deactivation of Rac1 (Supplemental Figure 4B). To more directly assess the effect of laminin-332 on Rac1 activity, we proceeded to measure the Rac1 activity of leaders and singles upon interaction with purified human laminin-332. Surprisingly, laminin-332 only led to Rac1 activation in single cells, while Rac1 activity remained unchanged in leaders (Figure 5D). Similar to purified laminin-332, treatment of leaders and singles to laminin-332-rich leader CM only led to activation of Rac1 in singles, while a gradual deactivation of Rac1 was observed in leaders (Figure 5E). Furthermore, treatment of singles with CM from *Lama3* WT and two

Lama3 KO leader clones yielded significantly higher Rac1 activity upon treatment with leader *Lama3* WT CM when compared to the leader *Lama3* KO CM after 10 minutes (Figure 5F). To confirm that the secretome of *Lama3* WT and KO cells are similar (other than Lama3 protein), we performed mass spectrometry-based proteomic analysis of the CM of these cells and found only 33 differentially abundant proteins (|Student's T-test Difference| > 1, $p<0.05$) out of 783 total proteins (LFQ Score < 10), including Lama3, which had the lowest p-value by a considerable margin (Supplementary Figure 4C). In addition, treatment of singles with *Lama3* WT leader CM with a laminin-332 polyclonal antibody led to a reversal of Rac1 activation, further confirming the direct effect of leader-derived laminin-332 on Rac1 activity in single cells amongst the complex mixture of molecules found in leader CM (Figure 5G).

To confirm that laminin-332 binds to the integrin α6/β4 receptor within singles to activate Rac1, we measured the Rac1 activity of singles with *Itga6* knockdown (Figure 5G). When unstimulated, we observed no difference in Rac1 activity between vehicle and the knockdown cells (Figure 5H). Upon stimulation with *Lama3* WT leader CM, however, we found that only the vehicle cells were able to activate Rac1, while the knockdown cells retained the same Rac1 activity as the unstimulated cells (Figure 5H). Additionally, we observed a significant decrease in Rac1 activity in shItga6 singles upon treatment leader *Lama3* KO CM relative to the leader *Lama3* WT CM, confirming the importance of both laminin-332 and integrin α6 for Rac1 activity in single cells (Figure 5H). Taken together, these data support a model whereby single cells utilize integrin α6/β4 receptor binding to laminin-332 derived from collectively-invading cells for Rac1 activation.

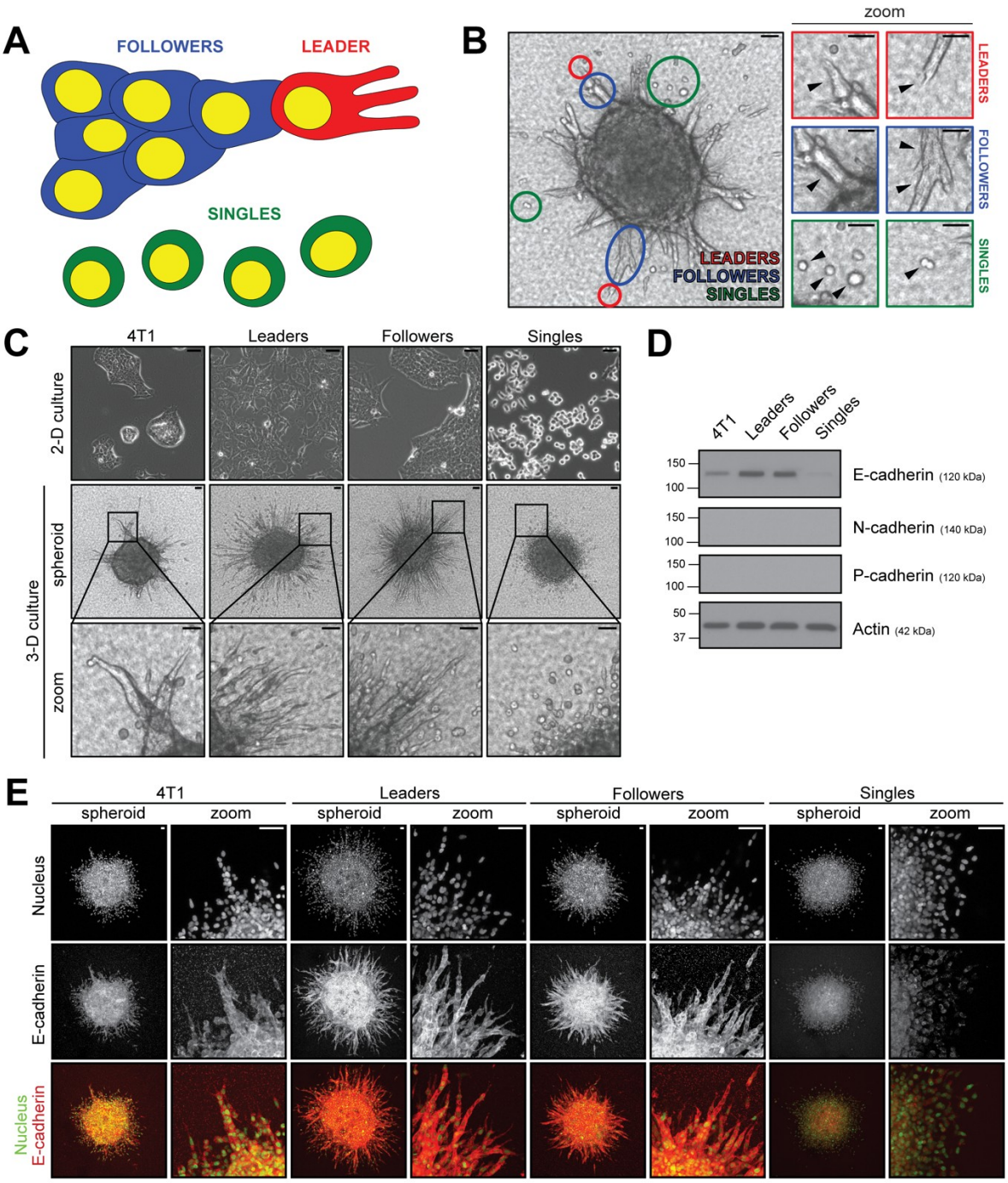

Figure 1. Subpopulations derived from the invasively heterogeneous 4T1 cell line are morphologically distinct. (A) Schematic detailing the criteria by which leaders, followers and

singles would be identified and isolated via SaGA. **(B)** Brightfield image (10X) of a 3-D 4T1 parental spheroid embedded in 3.0 mg/mL rat-tail collagen type I after 24 h. Select leaders, followers, and singles are encircled with a red, blue and green circle, respectively, and zoomed in. Scale bar, 50 μm. **(C)** Brightfield images of 4T1 parentals and purified leaders, followers and singles in 2-D (20X) and 3-D culture (10X). Scale bar, 50 μm. **(D)** Protein levels of E-cadherin, N-cadherin, and P-cadherin in whole cell lysates of 4T1 parentals, leaders, followers and singles. Actin was used as a loading control. **(E)** Immunofluorescence images of E-cadherin, N- on 3-D spheroids of 4T1 parentals, leaders, followers and singles at 1.25x zoom (left) and 5.0x zoom (right). Images were acquired at 10X magnification. Yellow in the overlay image denotes nuclei fluorescence emitted from H2B-Dendra2 and red denotes E-cadherin staining. Scale bar, 50 μm. For (D) and (E), three biological replicates were performed.

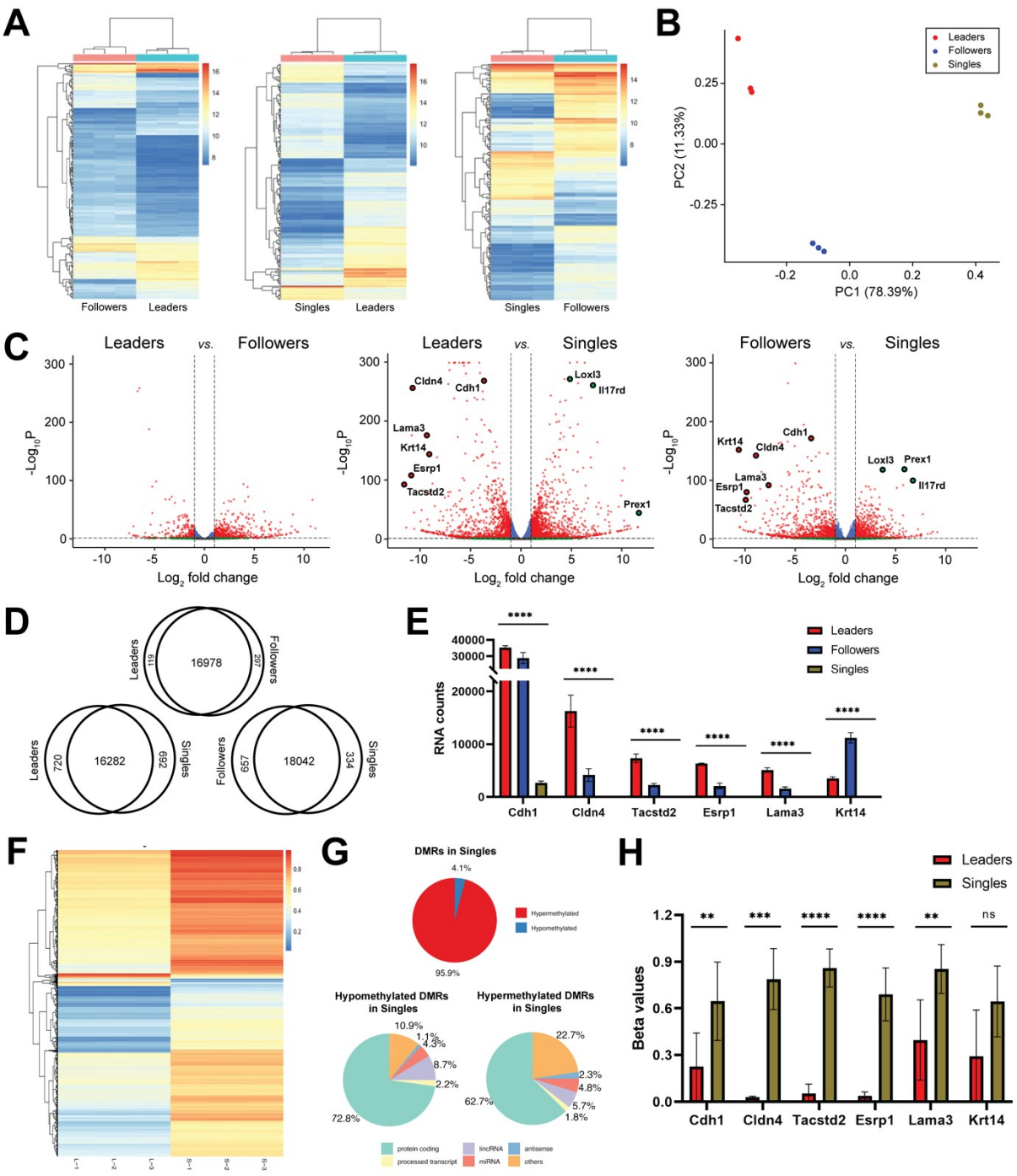

Figure 2. Collectively-invading and single cells exhibit distinct transcriptional and epigenetic programs. (A) Heat maps from RNA sequencing data for each pair-wise comparison. Scale denotes z scores from log2-normalized expression counts of most differentially expressed

genes. **(B)** Principal component analysis (PCA) plot of leaders, followers and singles based on RNA sequencing data (n=3). **(C)** Volcano plots denoting differentially expressed genes (DEGs) for each pair-wise comparison. DEGs (small, unbordered red dots) were classified as gene transcripts with $-Log_{10}P$ values of greater than 1.3 (y-axis) and a log2 fold change difference of greater than 2.0 or less than -2.0 (x-axis). Bordered red dots are select genes over-expressed in collectively-invading cells and bordered green dots are select genes over-expressed in single cells. **(D)** Number of DEGs between each pair-wise comparison. **(E)** RNA counts for *Cdh1, Cldn4, Tacstd2, Esrp1, Lama3* and *Krt14* in leaders, followers and singles (n=3). **(F)** Heat map of mouse methylation beta values between leaders and singles and representation of the percentage of hypermethylated regions across all differentially-methylated regions (DMR) between leaders and singles. Scale on heat map denotes beta value difference values for each DMR. L-1, L-2, L-3 denotes three replicates of leaders and S-1, S-2, and S-3 denotes three replicates of singles. **(G)** Annotation of DMRs in singles when compared to leaders. **(H)** Beta value comparison of CpG loci within the promoter region of *Cdh1* (n=7)*, Cldn4* (n=4)*, Tacstd2* (n=5)*, Esrp1* (n=6)*, Lama3* (n=7) and *Krt14* (n=3) between leaders and singles. For all panels: mean ± SEM is shown. Unless noted, n.s., no significance, ** $p \leq 0.01$, *** $p \leq 0.001$, **** $p \leq 0.0001$.

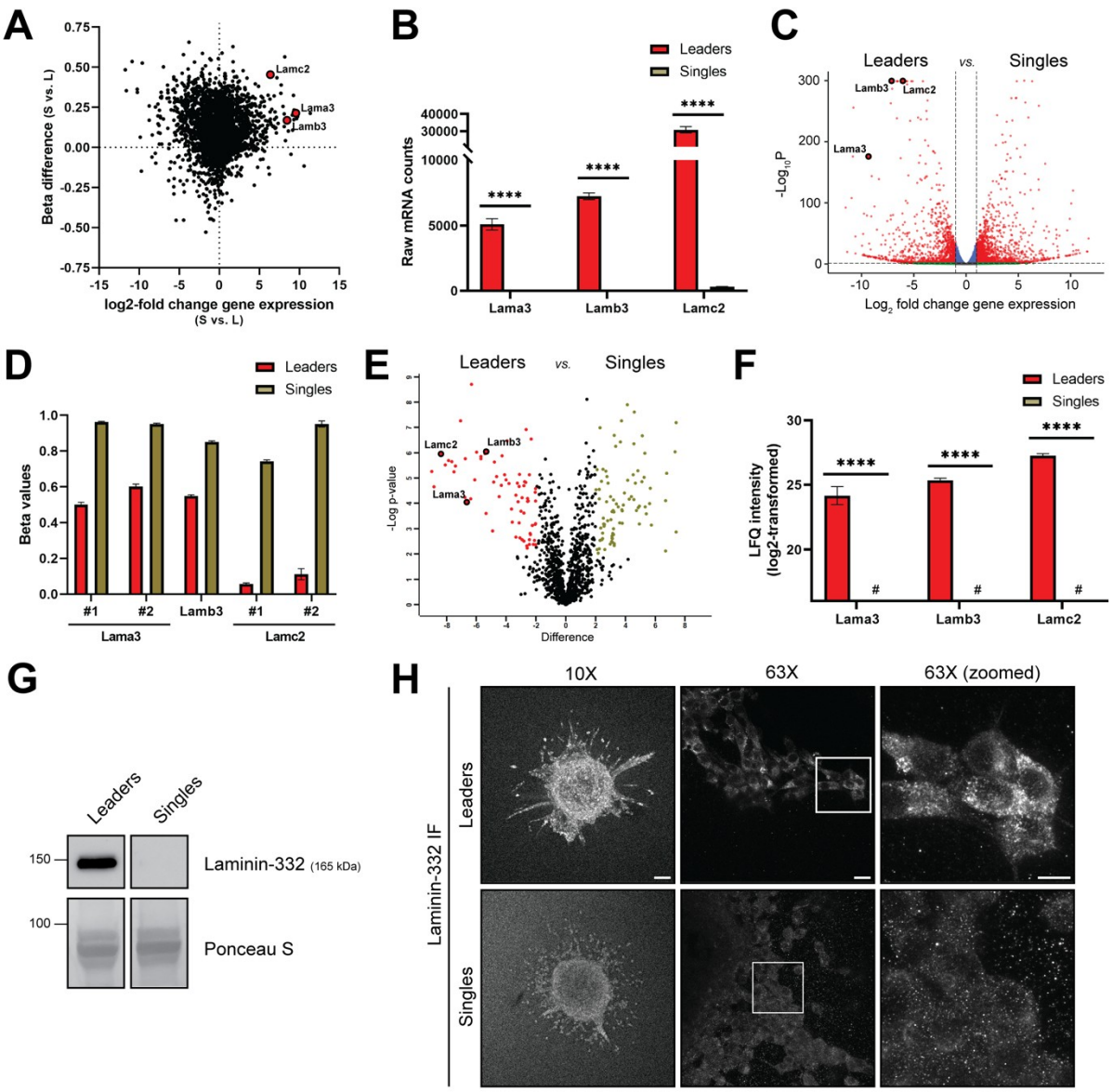

Figure 3. Collectively-invading cells over-express and abundantly secrete laminin-332. (A) Integration of RNA sequencing log2 fold change values (x-axis) and mouse methylation array beta difference values (y-axis) for the leaders vs. singles pair-wise comparison. *Lama3*, *Lamb3* and *Lamc2* are highlighted as red dots among gene transcripts with high mRNA transcription in leaders and significant hypomethylation at the promoter region compared to singles. **(B)** Raw mRNA counts for gene transcripts of the laminin-332 subunits from RNA sequencing analysis

(n=3, **** p<0.0001). **(C)** Volcano plot of the leaders vs. singles pair-wise comparison derived from RNA sequencing data highlighting *Lama3*, *Lamb3* and *Lamc2* (bordered red dots) as prominent DEGs. **(D)** Beta value comparison of distinct CpG loci within the promoter regions of *Lama3*, *Lamb3* and *Lamc2* between leaders and singles. **(E)** Volcano plot of differentially secreted peptides extracted via LC-MS/MS from conditioned media from leaders and singles. Red, unbordered dots denote peptides differentially secreted in leaders and green dots denote peptides differentially secreted in singles. **(F)** LFQ intensity quantification of Lama3, Lamb3 and Lamc2 peptides. # denotes an absence of signal detected (n=3, **** p<0.0001). **(G)** Protein levels of laminin-332 in leaders conditioned media (CM) and singles CM. Total protein staining via Ponceau S was used as a loading control. **(H)** Laminin-332 immunofluorescence staining on invasive leaders and singles in collagen I 3-D culture (10X and 63X). Scale bar: 100 μm for 10X image, 20 μm for 63X image, and 10 μm for 63X zoomed image. For all panels: mean ± SEM is shown. For (G) and (H), three biological replicates were performed.

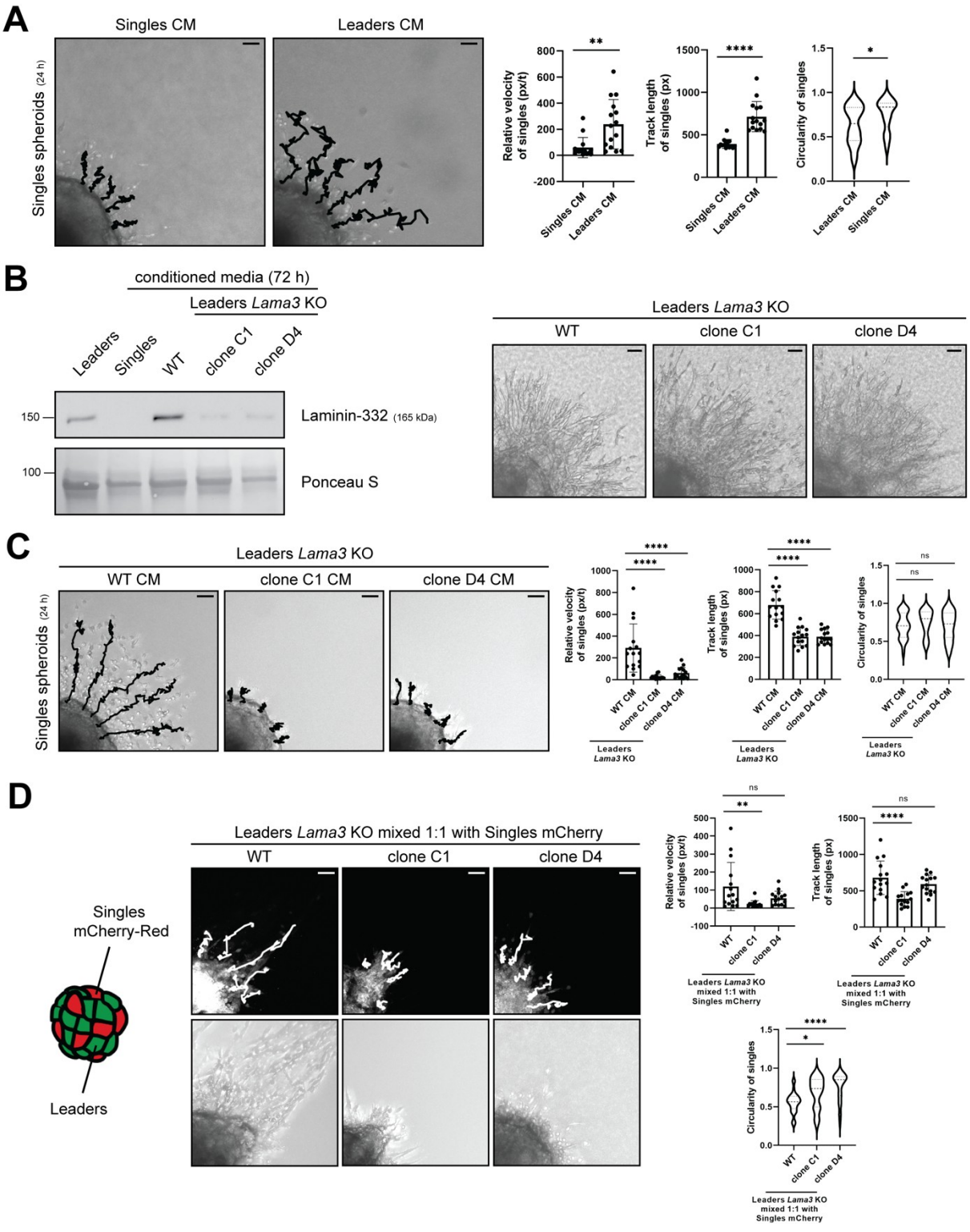

Figure 4. Laminin-332 enhances the invasive potential of singles. (A) Live-cell tracking

analysis of singles spheroids after treating with singles CM or leaders CM for 24 h (n=15). Representative five tracks highlighted for each group. Scale bar, 50 μm. **(B)** Protein levels of laminin-332 in conditioned media extracted from leaders with wildtype *Lama3* (WT), and *Lama3* CRISPR/Cas9 knockout (clones C1 and D4). Total protein staining via Ponceau S was used as a loading control. Brightfield images were acquired after 24 h. Scale bar, 50 μm. **(C)** Live-cell tracking analysis of singles spheroids after treating with conditioned media from wildtype *Lama3* leaders (WT) and *Lama3* knockout leaders (clones C1 and D4) (n=15). Representative five tracks highlighted for each group. Scale bar, 50 μm. **(D)** Live-cell tracking analysis of mCherry-transfected singles within a spheroid mixed 1:1 with mCherry-transfected singles and either leaders WT, clone C1 or clone D4 (n=15). Representative five tracks highlighted for each group. Scale bar, 50 μm. For all experiments, three biological replicates were performed. For all panels: mean ± SEM is shown. Unless noted, n.s., no significance, * $p \leq 0.05$, ** $p \leq 0.01$, *** $p \leq 0.001$, **** $p \leq 0.0001$.

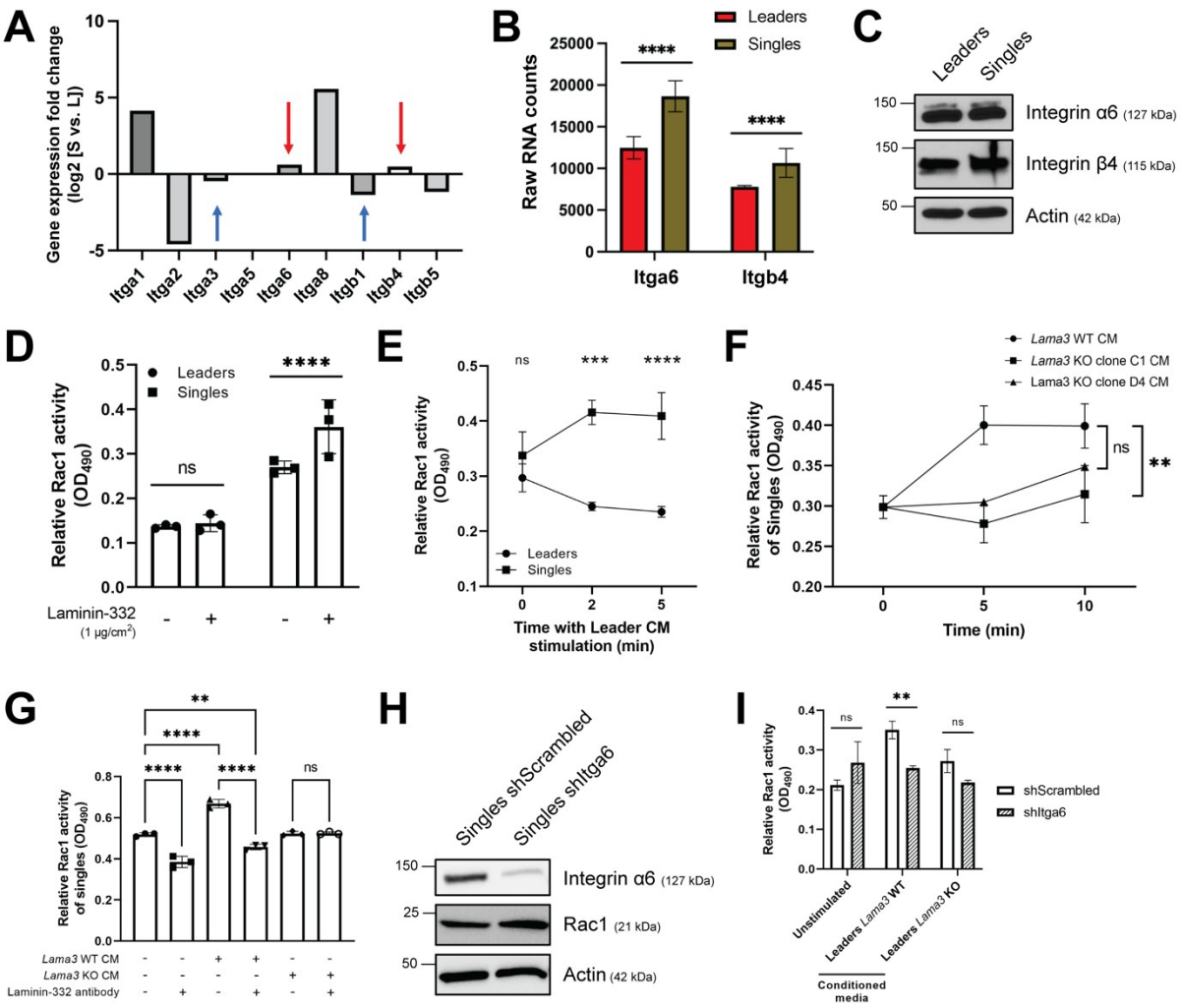

Figure 5. Singles activate Rac1 activity via binding of integrin α6β4 to leader-derived laminin-332. (A) Log_2 fold change of integrin subunits expressed in leaders and singles within the RNA sequencing data. Positive values denote gene transcripts that were upregulated in singles relative to leaders. Red arrows highlight *Itga6* and *Itgb4* as being upregulated in singles and blue arrows highlight *Itga3* and *Itgb1* as being downregulated in singles. **(B)** RNA counts for *Itga6* and *Itgb4* in leaders and singles (n=3). **(C)** Protein levels of integrin α6 and β4 in whole cell lysates of leaders and singles. Actin was used as a loading control. **(D)** Relative Rac1 activity of leaders and singles upon direct interaction with 1 μg/cm^2 laminin-332 for 5 minutes

(n=3). **(E)** Time course measurement of relative Rac1 activity in leaders and singles upon leader CM treatment (n=3). **(F)** Time course measurement of relative Rac1 activity in singles upon treatment with CM from leaders *Lama3* wildtype (WT) and 2 distinct leaders with *Lama3* KO (clone C1 and clone D4) (n=3). Statistical annotation only applies for the 10 minute time point. **(G)** Relative Rac1 activity of singles upon treatment with *Lama3* WT or *Lama3* KO CM with a laminin-332 antibody (1:1000 dilution) (n=3). Laminin-332 antibody was mixed in with CM for 30 minutes prior to treatment. Rac1 activity of cells was measured after 5 minute treatment with CM. **(H)** Protein levels of integrin α6 and total Rac1 upon *Itga6* shRNA knockdown in singles. Actin was used as a loading control. **(I)** Relative Rac1 activity in singles with *Itga6* shRNA knockdown (shItga6) upon treatment with conditioned media from leaders *Lama3* WT and leaders *Lama3* KO. Rac1 activity was measured after 1 h treatment with CM (n=3). For (C), (D), (E), (F), (G), (H) and (I), three biological replicates were performed. For all panels: mean ± SEM is shown. Unless noted, n.s., no significance, ** $p \leq 0.01$, *** $p \leq 0.001$, **** $p \leq 0.0001$.

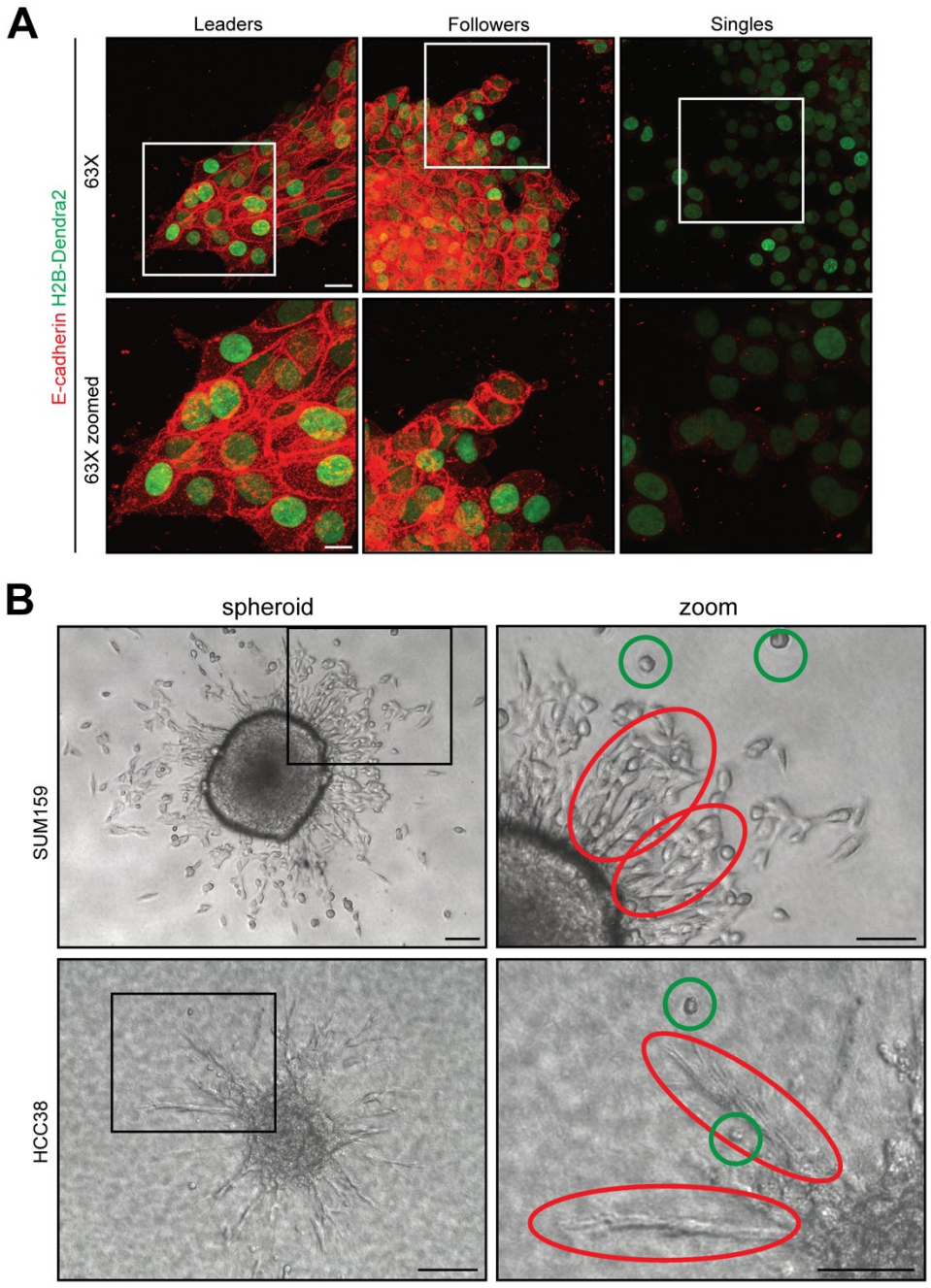

Supplementary Figure 1. Human triple-negative breast cancer cell lines are invasively heterogeneous. (A) High magnification images (20x and 63x) of E-cadherin immunofluorescence on 3-D spheroids of 4T1 leaders, followers and singles. Green in the overlay image denotes nuclei fluorescence emitted from H2B-Dendra2 and red denotes E-

cadherin staining. Scale bar, 50 μm. **(B)** Brightfield image of a SUM159 (10X) and HCC38 (20X) spheroid embedded in rat-tail collagen type I after 24 h invasion. Red circles denote collective chains and green circles denote single cells. Scale bar, 50 μm.

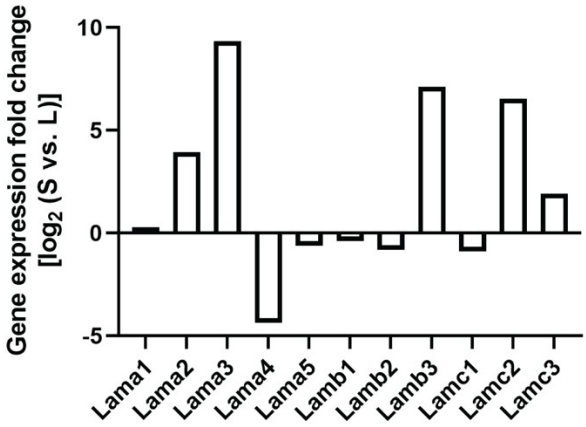

Supplementary Figure 2. Fold change difference of laminin gene expression between leaders and singles.

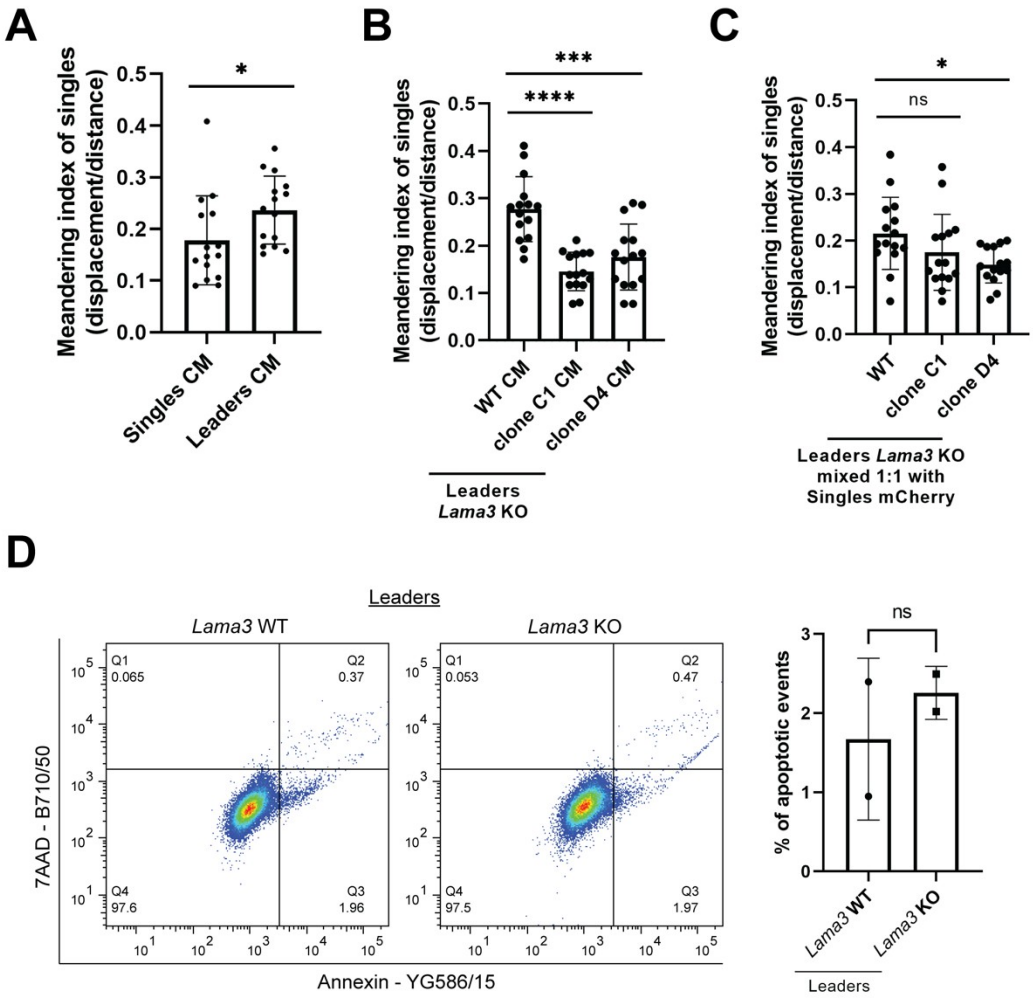

Supplementary Figure 3. Lama3 KO does not affect leader cell viability and suppresses directional movement of single cells. (A-C) Meandering index quantification for singles (A) treated with leader or singles conditioned media (CM), (B) *Lama3* knockout leaders CM, and (C) mixed 1:1 with *Lama3* knockout leaders (n=15). **(D)** Quantification of apoptotic events on leaders with *Lama3* wildtype (WT) and knockout (KO) (n=2). For all panels: mean ± SEM is shown. Unless noted, n.s., no significance, * $p \leq 0.05$, *** $p \leq 0.001$, **** $p \leq 0.0001$.

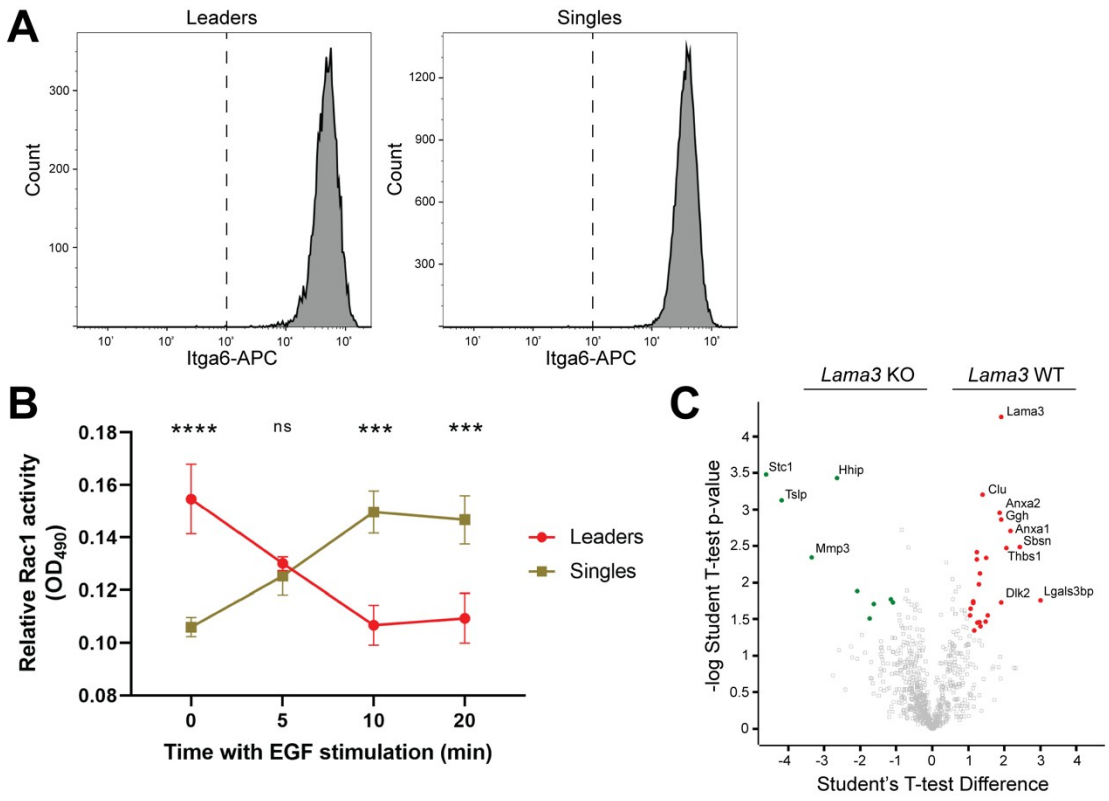

Supplementary Figure 4. EGF activates Rac1 in single cells and not collectively invading cells. (A) Flow cytometric surface protein quantification of integrin α6 (Itga6) in leaders and singles. Dotted line denotes the unstained sample for each subpopulation. **(B)** Time course measurement of relative Rac1 activity in leaders and singles upon 50 ng/mL hEGF treatment (n=3, *** $p<0.001$, **** $p<0.0001$). Mean ± SEM is shown. **(C)** Volcano plot of differentially secreted peptides extracted via LC-MS/MS from conditioned media from leaders with *Lama3* wildtype (WT) and knockout (KO) (n=3). Red circles denote peptides differentially secreted in *Lama3* WT leaders and green circles denote peptides differentially secreted in *Lama3* KO leaders (|Student's T-test Difference| > 1, p-value < 0.05).

Marker Analysis

Marker Name	Parentals		Leaders		Followers		Singles	
	Sample Results	4T1 (ATCC# CRL-2539)	Sample Results	4T1 (ATCC# CRL-2539)	Sample Results	4T1 (ATCC# CRL-2539)	Sample Results	4T1 (ATCC# CRL-2539)
MCA-4-2	21.3	21.3	21.3	21.3	21.3	21.3	21.3	21.3
MCA-5-5	14	14	14	14	14	14	14	14
MCA-6-4	18	18	18	18	18	18	18	18
MCA-6-7	12	12	12	12	12	12	12	12
MCA-9-2	15	15	15	15	15	15	15	15
MCA-12-1	16	16	16	16	16	16	16	16
MCA-15-3	22.3	22.3	22.3	22.3	22.3	22.3	22.3	22.3
MCA-18-3	18, 19	18, 19	18, 19	18, 19	18	18, 19	18, 19	18, 19
MCA-X-1	25	25	25	25	25	25	25	25

Supplementary Table 1. Single tandem repeat (STR) analysis of 4T1 parentals, leaders, followers, and singles. Nine genomic markers spanning eight chromosomes are compared between the isolated subpopulations and the ATCC 4T1 cell line.

Supplementary Table 1. Single tandem repeat (STR) analysis of 4T1 parentals, leaders, followers, and singles. Nine genomic markers spanning eight chromosomes are compared between the isolated subpopulations and the ATCC 4T1 cell line.

2.6 Discussion

Despite the prevalence of phenotypic heterogeneity across multiple solid tumor types, the mechanisms underlying invasively distinct subpopulations remain largely unexplored. Using SaGA, we isolated and analyzed both collectively-invading cells (leaders and followers) and individually-invading cells (singles) within the 4T1 murine mammary adenocarcinoma model. We performed RNA sequencing on these purified cell subpopulations to investigate transcriptional differences and found that collectively-invading and single cells had vastly different transcriptomes that includes upregulation of key epithelial genes such as *Cdh1*, *Krt14*, *Esrp1*, *Cldn4* and *Tacstd2* in collectively-invading cells. E-cadherin (*Cdh1*) was only expressed in collectively-invading cells and not single cells, which has been observed previously (*120*), and is required for metastasis in multiple breast cancer models (*141*). Similarly, Keratin-14 (*Krt14*) is also a well-characterized biomarker for breast cancer leader cells within collective packs (*115, 142*) and had significantly higher expression in collectively invading cells compared to singles. Furthermore, keratin-14 knockdown has previously been shown to abrogate the ability for cells to invade collectively and form clustered metastases (*115*). The relevance of *Esrp1*, *Cldn4* and *Tacstd2* within collectively-invading cells is less characterized, but they have been shown to drive cell invasion in multiple tumor models (*143, 144, 145*). In contrast to collectively-invading cells, cells that exclusively invade as single cells exhibited very low levels of canonically epithelial genes, including *Cdh1*, *Esrp1*, and *Tacstd2*, suggesting that single cells may represent a hybrid amoeboid state within the epithelial-to-mesenchymal transition (EMT) program (*46*). Additionally, Gene Ontology on single cells showed statistically significant enrichment of multiple EMT-related pathways, including *Regulation of epithelial to mesenchymal transition* (GO:0010717) and *Epithelial to mesenchymal transition* (GO:0001837). The phenotypic

persistence of single cells over multiple passages would suggest that single cells (and collectively-invading cells) are not in active transition within this spectrum, but the influence of related pathways to their single-cell phenotype cannot be ruled out.

Subsequent methylation analyses revealed that collectively-invading and single cell subpopulations exhibit significant epigenetic differences. Interestingly, gene transcripts with the highest fold changes in RNA expression between collectively-invading and single cells also had prominent differences in methylation patterns at both the promoter regions and gene bodies of the corresponding genes, including *Cdh1*, *Krt14*, *Esrp1*, *Cldn4, Tacstd2* and *Lama3*. An epigenetic basis for the emergence of collectively-invading and single cells is supported by the stability we observe in the distinct phenotypes between collectively-invading and single cell subpopulations throughout multiple passages. The stability of these distinct phenotypes could also be attributed to genomic differences between the subpopulations. Although STR analysis of 9 genomic markers revealed no prominent differences between these subpopulations (Supplementary Table 1), we cannot rule out a possible role for an underlying genomic heterogeneity governing these distinct phenotypes. Despite this, our data provide support for collectively-invading cells and single cells having distinct epigenetic programs that shape their distinct transcriptional profiles to influence cellular phenotype.

Integration of RNA sequencing and methylation data identified gene transcripts of components of the laminin-332 trimeric complex—*Lama3*, *Lamb3*, and *Lamc2*—as being highly overexpressed and hypomethylated in collectively-invading cells relative to single cells. Furthermore, unbiased secretomic analysis confirmed that components of the laminin-332 complex were being exclusively secreted by collectively-invading cells. In healthy skin, laminin-332 is specific to the basement membranes of epithelial tissue, and is normally produced and

secreted by keratinocytes to bolster cell survival and play a role in wound healing (*146, 147, 148*). Similarly, cancer cells of epithelial origin have been found to abnormally express laminin-332 to promote anoikis resistance and induce cell motility (*149, 150*). Recent work established the relevance of laminin-332 within collective invasion, largely focusing on its role in establishing cell-cell contacts within focal adhesions across collective chains (*151*). In healthy skin, the integrin α6β4 heterodimer in epithelial cells and laminin-332 in the underlying basement membrane bind to maintain hemidesmosome integrity across highly structured epithelial tissue (*140, 152*). Interestingly, we show that laminin-332 can also bind to integrin α6β4 as a secreted factor when integrin α6β4 is expressed in a spatially distant cell. Our work corroborates recent discoveries identifying laminin-332 as a factor secreted by collectively-invading cells, further clarifying the role of laminin-332 in triple-negative breast cancer invasion (*153*).

Interestingly, collectively-invading cells and single cells had similar protein expression of the integrin α6β4 heterodimer, suggesting that laminin-332 binding to single cells is likely not an exclusively paracrine interaction. Autocrine laminin-332 binding has been reported in skin squamous cell carcinoma and mammary tumor models, wherein laminin-332 binding to syndecan-1 or EGFR leads to further laminin-332 deposition in a positive-feedback loop (*149, 154, 155*). Despite this, we show that one downstream target of integrin α6β4, Rac1, is exclusively activated in singles upon treatment with purified laminin-332 (Figure 5D) and laminin-332-rich conditioned media derived from collectively-invading cells (Figure 5E). Current work supports multiple possible explanations for this duality in Rac1 activation, including mutations or splice variants of either integrin α6 or β4. Instances of such mutations within the *ITGB4* genes have been reported in cases of epidermolysis bullosa, wherein the

mutations are predicted to reduce integrin α6β4 heterodimer stability (*156*). Additionally, splice variants of integrins α6 and β4 that affect proper dimerization and cell membrane anchoring have been reported with different downstream targets such as ERK and JNK (*157, 158*). Further investigation is required to elucidate the stark differences in Rac1 activity stimulation between collectively-invading cells and single cells despite similar membrane-bound integrin α6 and β4 expression.

Our work explores the intricacies of phenotypic heterogeneity within triple-negative cancer and unravels a commensal interaction between phenotypically-distinct cancer subpopulations. The attribution of ecological relationships to subpopulation cellular dynamics has been of recent interest, namely in the identification of cooperative interactions between subpopulations of heterogeneous cancer cell lines (*27, 28, 87, 159*). Thus far, breast cancer cells cooperate through leader-follower dynamics within collectively-invading chains to overcome energetic barriers presented by dense collagen matrices through perpetual "shuffling" of leader and follower cells (*30*). Additionally, lung adenocarcinoma models have profound increases in cell survival and DNA repair within highly dynamic leaders through secreted factors found in follower conditioned media (*27*). More recent evidence has revealed the advantage cooperating clustered cells have as opposed to individual invasive cells in overcoming immune attack from natural killer cells (*118*). Our work describes a commensal relationship, wherein collectively-invading cells confer a unilateral invasive benefit unto single cells. To our knowledge, this represents a novel commensal interaction between cancer cell subpopulations, amidst extensive work that has characterized commensal interactions between the gut or skin and their respective microbiota (*160, 161, 162*). We speculate that Rac1 activation in singles due to laminin-332 binding could be one aspect of a cooperative effort between collectively-invading cells and

single cells, but further work is necessary to test the model that actively invasive single cells benefit collectively-invading cells to enhance the metastatic potential of a heterogeneous tumor.

In summary, we isolated and characterized collectively-invading and single cells within a highly heterogeneous murine triple-negative breast cancer model and discovered the secretion of the laminin-332 complex exclusively by collectively-invading cells. We show that laminin-332 derived from collectively-invading cells enhances the invasive potential of singles and also stimulates the Rac1 activity of singles. Through this mechanism, we suggest that collectively-invading and single cells display a commensal relationship, wherein collectively-invading cells unidirectional benefit single cells. This commensal relationship does not exclude the possibility for additional work revealing a mutualistic relationship wherein both populations benefit one another. Our work contributes towards a more complete understanding of how phenotypic heterogeneity and subpopulation dynamics precedes cell invasion and metastatic progression, which we anticipate will be crucial to developing personalized treatments against this ever-evolving heterogeneous disease.

Chapter 3: Discussion and Future Directions

3.1. Collectively-invading cells and single cells are phenotypically-distinct subpopulations

Collectively-invading cells and single cells have been observed to co-exist in primary breast tumors in both mice and humans, but the mechanistic implications of this co-existence have yet to be explored (*74, 75, 76*). Here, we find that collectively-invading cells and single cells that emerge from the 4T1 mammary adenocarcinoma cell line are distinct subpopulations with persistent cell morphologies and invasive behaviors (Figure 1C). The prominent phenotypic differences of these cell subpopulations allow for them to be isolated using Spatiotemporal Genomic and Cellular Analysis (SaGA) for transcriptional and epigenetic characterization (*61*). Interestingly, very minimal shifting of cell phenotypes are observed within these subpopulations over multiple passages. This suggests that collectively-invading and single cells are not in a transitive cell states that are highly susceptible to phenotype switching. This observation is of interest, as cell transitions such as EMT have classically been considered to be an important step for cancer cells to progress into a more malignant state (*48, 49*). Our work supports a more current understanding that subpopulations such as collectively-invading and single cells represent a more "differentiated" cell type that is not merely a stage en route to becoming a more malignant cancer cell.

Collectively-invading cells represent a highly invasive subpopulation that depends on adherent cell-cell junctions for cell movement (*24*). In breast cancer, collectively-invading chains consist of leader and follower cells that alternate in leading the chain to more effectively overcome energy barriers posed by dense stroma (*30*). Due to this alternating dynamic between these subpopulations in collective chains, leader and follower cells in breast cancer cells cannot be isolated purely based on spatial parameters, as in non-small cell lung adenocarcinoma cells.

As such, we acknowledge that leader and follower cells that were isolated through SaGA like represent a mixed population of both leader and follower cells. Thus, we proceeded to use leaders as a representative for collectively-invading cells in the majority of experiments here, especially considering the transcriptomic similarities between the two isolated subpopulations (Figure 2D). Relative to single cells, we find that collectively-invading cells express high levels of E-cadherin and no expression of N-cadherin or P-cadherin (Figure 1D). The reliance on E-cadherin for collective invasion suggests that collectively-invading cells exhibit epithelial characteristics despite being highly motile. This is further supported by high expression of epithelial program modulators such as *Esrp1* and *Tacstd2* and other common epithelial markers such as *Cldn4* and *Krt14* in collectively-invading cells (Figure 2C) (*144, 145, 163, 164*). The lack of N-cadherin expression also suggests that collectively-invading may not align with mesenchymal phenotypes despite exhibiting mesenchymal-like invasive properties, such as robust filopodia-dependent cell movement and spindle-like morphology (*38*).

In contrast to collectively-invading cells, single cells represent a highly flexible subpopulation that does not depend on cell-cell junctions for cell movement (*24*). In particular, the rounded shape of single cells in both 2-D and 3-D suggests that the single cell subpopulation in 4T1 cells is predominantly amoeboid morphologically (Figure 1C) (*43, 46*). Despite this, transcriptomic analysis of single cells revealed enrichment in gene sets associated with EMT, which suggests that single cells may represent a more mesenchymal phenotype transcriptionally despite an amoeboid morphology. Single cells exhibiting higher RNA and protein expression of the classically mesenchymal marker vimentin supports this (data not shown), despite vimentin also being implicated in promoting amoeboid movement in cancer cells (*165*). This suggests that single cells could potentially have transitioned from more epithelial-like cells through loss of

cell-cell junctions and now represents a hybrid phenotype between mesenchymal and amoeboid profiles. The persistent phenotype of single cells and their stringent inability to invade in chains would suggest that this early transition is largely irreversible and restricted to early stages of tumor invasion. Whether a particular stimulus drives this transition or if it is a consequence of phenotypic heterogeneity remains unclear.

3.2. Collectively-invading cells over-express laminin-332

Integration of transcriptomic and DNA methylation analyses revealed a stark over-expression of laminin-332 components in collectively-invading cells relative to single cells (Figure 3A). This over-expression was further validated through an unbiased proteomic analysis of conditioned media from collectively-invading cells (Figure 3C), and also through targeted antibody-based methods, including immunoblotting of conditioned media (Figure 3G) and 3-D immunofluorescence (Figure 3H). Laminin-332 over-expression has been commonly observed in solid tumors and has largely been correlated with poor clinical prognosis and tumor progression (*140, 155, 166*). Despite these correlations, laminin-332 expression is not specific to cancer cells —laminin-332 is a prominent component of basement membranes in healthy epithelial tissues is actively secreted by keratinocytes (*140, 146*). Furthermore, laminin-332 mediates hemidesmosome integrity when localized to the cell membrane as a transmembrane glycoprotein (*140*). Through 3-D immunofluorescence, we show that laminin-332 is actively localized both in the cell membrane, endoplasmic reticulum, and in vesicles, suggesting that laminin-332 is being actively secreted through vesicular release, and potentially playing a role in hemidesmosomes between collectively-invading cells (Figure 3H). Interestingly, immunofluorescence staining of collectively-invading cells does not capture staining of extracellular laminin-332. Laminin-332

staining in 3-D spheroids has previously been observed to resemble a halo around the spheroid, but these observations were made weeks after initial seeding in agarose gels (*167*). Staining of such laminin-332 deposition in collectively-invading 4T1 cells embedded in collagen pose a technical challenge due to the highly aggressive nature of the 4T1 cell line. Additionally, embedding 4T1 spheroids in agarose resulted in significant cell death within days of embedding (data not shown), further limiting the ability to image extracellular laminin-332 within 4T1 spheroids.

Despite the prevalence of laminin-332 expression in solid tumors, the link between laminin-332 and collective invasion is not well established. Laminin-332 has been found to be important in establishing cell-cell junctions between collectively-invading cells and promoting "contact following"—the phenomenon wherein cells move in the same direction mediated by intercellular adhesion—in epidermoid carcinoma cells (*151*). We find, however, that loss of laminin-332 through *Lama3* CRISPR/Cas9 knockout does not abrogate the ability for cells to invade as adherent cells, suggesting that the laminin-332 complex may not be as critical for cell-cell adhesion in 4T1 collectively-invading cells considering the expression of other adhesion proteins such as E-cadherin and other claudins (Figure 4B). Laminin-332 has also been found to be secreted by collectively-invading cells in multiple triple-negative breast cancer cell models, wherein laminin-332 secretion was downstream of Cdh3 signaling through β-catenin (*153*). Although Cdh3 expression was undetectable both transcriptionally and in protein within our 4T1 subpopulations (Figure 1D), these findings suggest that E-cadherin (Cdh1)-mediated signaling could impact laminin-332 expression in a similar manner within 4T1 cells. Further investigation is necessary to more comprehensively understand the molecular link between E-cadherin and laminin-332 in collectively-invading cells.

3.3. Laminin-332 activates Rac1 single cells

Through conditioned media treatment experiments, we show that the over-expression and secretion of laminin-332 by collectively-invading cells has profound effects on the nearby single cells (Figure 4A-C). Notably, we find that laminin-332 enhances both the velocity and directionality of movement in single cells (Figure 4C). Due to limitations in the ability to image extracellular laminin-332 in 3-D, it is inconclusive whether single cells bind to laminin-332 complexes that have polymerized or adhered to the collagen matrix or soluble laminin-332 components in the media. The nature of conditioned media experiments would suggest that the spheroids would be interacting with soluble laminin-332 components, but the capability for soluble laminin-332 components to adhere and deposit into the polymerized collagen matrix throughout the duration of live cell imaging (i.e. 24-48 hours) is largely unknown. Despite this gap in understanding, the effect of laminin-332 on single cells is robust, as exemplified by the mitigated effect of conditioned media generated from collectively-invading cells with *Lama3* knocked out (Figure 4C). Furthermore, our mixed spheroid experiments wherein singles tagged with mCherry are combined with collectively-invading cells within the same spheroid show that these findings can be replicated in a model that recapitulates the physical proximity of heterogeneous cell subpopulations within a single tumor (Figure 4D).

The activation of cell velocity and directionality in single cells upon laminin-332 binding led us to investigate whether Rac1 was involved downstream of this interaction. We show that laminin-332 derived from collectively-invading cells is sufficient to activate Rac1 in singles, and that this activation is more robust in singles relative to collectively-invading cells (Figure 5E). Furthermore, we show that integrin $\alpha 6$ is required for laminin-332-induced Rac1 activation in

single cells (Figure 5I). The binding of laminin-332 to integrin α6β4 has been shown to activate Rac1 in keratinocytes, which originally depend on RhoA activation for cell movement during wound healing (*140, 149*). The deposition of laminin-332 by these keratinocytes results in a gradual switching to Rac1 activation as these migratory cells begin to bind laminin-332 with integrin α6β4 (*140*). This GTPase activation switch from RhoA to Rac1 results in cells with higher directionality and invasion modalities that depend more on cell-cell adhesion (*24*). Interestingly, single cells also demonstrated higher directionality in movement and became less rounded morphologically upon laminin-332 exposure (Figure 4C, Supplementary Figure 3B). This suggests that singles, like keratinocytes, may originally activate RhoA to maintain their amoeboid phenotype and relatively higher stochastic movement, but switch to activate Rac1 upon laminin-332 binding to mirror the directional movement of collectively-invading cells.

It remains unknown the direct consequences of this increased cell invasion and directionality in single cells upon laminin-332 binding within the context of a heterogeneous cancer cell pool. The mirroring of directional movement between collectively-invading cells and single cells after laminin-332 binding may suggest a type of "cellular influencing" towards more spindle-like collective invasion, which represents the more effective mode of metastatic dissemination (*32, 33*). This would support a commensal interaction wherein collectively-invading cells unilaterally provide higher metastatic fitness to single cells. It also remains a possibility that single cells could bolster collectively-invading cells as a response to this elevated directionality and velocity through the secretion of matrix-modifying proteins, growth factors, or other proteins that support robust collective invasion. RNA sequencing in single cells revealed upregulation of collagen modifying and remodeling proteins relative to collectively-invading cells (data not shown), suggesting the potential for the more agile single cells to remodel

collagen structures ahead of collectively-invading cells to lower the energetic barriers required to invade through these stromal components. Such an interaction would support a cooperative relationship between these co-existing cancer subpopulations. Thus, further investigation is necessary to clarify the potential role of single cells within this model and the interactions between these heterogeneous cancer cell subpopulations.

3.4. Conclusions and future directions

In all, the work highlighted in this dissertation contributes towards the ongoing exploration of intercellular interactions between cancer subpopulations within heterogeneous cancer models. We show that phenotypically-distinct subpopulations can be isolated from heterogeneous cancer pools, and that these subpopulations retain their distinctive phenotypes over multiple passages. Furthermore, we show that the distinct morphologies of collectively-invading cells and single cells have both transcriptional and epigenetic underpinnings that are closely linked. Lastly, we show that these subpopulations do not merely co-exist, but interact through a laminin-332/Rac1 axis that provides a unilateral benefit to single cells. To our knowledge, this is the first characterization of a commensal relationship between cancer subpopulations. Considering the prevalence of these heterotypic interactions in cancer invasion and metastasis, the novelty of this work highlights the dire need for further identification and characterizations of these interactions. Despite tumor heterogeneity posing a significant obstacle for cancer treatment due to the diversity of subpopulations that exist within solid tumors, pharmaceutically hindering the interactions between these subpopulations has the potential to suppress the advantage tumor heterogeneity provides the tumor.

The novelty of this work sets the groundwork for more exploratory and pre-clinical investigation. The broad applicability of SaGA to a variety of solid tumors enables the isolation of phenotypically distinct subpopulations to more comprehensively understand the subpopulations that exist within heterogeneous tumors. Additionally, the multi-omic workflow presented in this work can be applied to other cancer subpopulations to uncover novel heterotypic interactions in metastatic tumors. The use of 4T1 cells in this work also enables a direct route to implanting these subpopulations into BALB/c mice (*168*). Investigating the prevalence of this commensal interaction between collectively-invading and single cells would provide a more complete understanding of the metastatic consequences of this interaction. Further work is also needed to explore whether Rac1 activation of single cells via laminin-332 occurs in other heterogeneous cell lines wherein collectively-invading and single cell subpopulations co-exist. Despite recent advances in cancer treatment and drastic improvements in patient prognosis for metastatic cancers, much remains unanswered regarding the intricacies of phenotypic heterogeneity on tumor metastasis. The work presented in this dissertation contributes a crucial step towards overcoming the seemingly insurmountable challenges posed by such an ever-evolving disease.

Chapter 4: References

1. Siegel, R. L., K. D. Miller, N. S. Wagle, and A. Jemal. 2023. Cancer statistics, 2023. *CA: a cancer journal for clinicians*. 73(1):17–48.
2. Cancer Facts & Figures 2023. Atlanta: American Cancer Society, Inc. 2022.
3. Harbeck N., F. Penault-Llorca, J. Cortes, M. Gnant, N. Houssami, P. Poortmans, K Ruddy, J. Tsang, F. Cardoso. 2019. Breast cancer. *Nat Rev Dis Primers*. 5(1):66.
4. Gerstberger, S., Q. Jiang, and K. Ganesh. 2023. Metastasis. *Cell*. 186(8):1564–1579.
5. Steeg P. S. 2016. Targeting metastasis. *Nat Rev Cancer*. (4):201-18.
6. Fidler I. J. 2003. The pathogenesis of cancer metastasis: the 'seed and soil' hypothesis revisited. *Nat Rev Cancer.* (3):453-458.
7. Pavlova, N. N., J. Zhu, and C. B. Thompson. 2022. The hallmarks of cancer metabolism: Still emerging. *Cell metabolism*. 34(3):355–377.
8. Subarsky P., R. P. Hill. 2003. The hypoxic tumour microenvironment and metastatic progression. *Clin Exp Metastasis.* (20):237-250.
9. Le Q. T., N. C. Denko, and A. J. Giaccia. 2004. Hypoxic gene expression and metastasis. *Cancer Metastasis Rev.* (23):293-310.
10. Chi, J. T., Z. Wang, D. S. Nuyten, E. H. Rodriguez, M. E. Schaner, A. Salim, Y. Wang, G. B. Kristensen, A. Helland, A. L. Børresen-Dale, A. Giaccia, M. T. Longaker, T. Hastie, G. P. Yang, M. J. van de Vijver and P. O. Brown. 2006. Gene expression programs in response to hypoxia: cell type specificity and prognostic significance in human cancers. *PLoS medicine*. 3(3):e47.
11. Blanco R. and H. Gerhardt. 2013. VEGF and Notch in tip and stalk cell selection. *Cold Spring Harb Perspect Med.* (3):a006569.

12. Boareto M., M. K. Jolly, E. Ben-Jacob and J. N. Onuchic. 2015. Jagged mediates differences in normal and tumor angiogenesis by affecting tip-stalk fate decision. *Proc Natl Acad Sci U S A*. (112):E3836-3844.
13. Rak J. W., B. D. St Croix, R. S. Kerbel. 1995. Consequences of angiogenesis for tumor progression, metastasis and cancer therapy. *Anticancer Drugs.* (6):3-18.
14. Rouhi, P., S. L. Lee, Z. Cao, E. M. Hedlund, L. D. Jensen and Y. Cao. 2010. Pathological angiogenesis facilitates tumor cell dissemination and metastasis. *Cell cycle (Georgetown, Tex.)*. 9(5):913–917.
15. Chang, J. and O. Chaudhuri. 2019. Beyond proteases: Basement membrane mechanics and cancer invasion. *The Journal of cell biology*. 218(8):2456–2469.
16. Kelley, L. C., L. L. Lohmer, E. J. Hagedorn and D. R. Sherwood. 2014. Traversing the basement membrane in vivo: a diversity of strategies. *The Journal of cell biology*. 204(3):291–302.
17. Greten, F. R. and S. I. Grivennikov. 2019. Inflammation and Cancer: Triggers, Mechanisms, and Consequences. *Immunity*. 51(1):27–41.
18. Dhatchinamoorthy, K., J. D. Colbert and K. L. Rock. 2021. Cancer Immune Evasion Through Loss of MHC Class I Antigen Presentation. *Frontiers in immunology*. (12):636568.
19. Ai, L., A. Xu and J. Xu. 2020. Roles of PD-1/PD-L1 Pathway: Signaling, Cancer, and Beyond. *Advances in experimental medicine and biology*. (1248):33–59.
20. Plaks V., C. D. Koopman, Z. Werb, 2013. Cancer. Circulating tumor cells. Science. (341):1186- 1188.

21. Chaffer C. L. and R. A. Weinberg. A perspective on cancer cell metastasis. *Science.* (331):1559- 1564.

22. Cameron, M. D., E. E. Schmidt, N. Kerkvliet, K. V. Nadkarni, V. L. Morris, A. C. Groom, A. F. Chambers and I. C. MacDonald. 2000. Temporal progression of metastasis in lung: cell survival, dormancy, and location dependence of metastatic inefficiency. *Cancer research*. 60(9):2541–2546.

23. Chambers A. F., G. N. Naumov, S. A. Vantyghem and A. B. Tuck. 2000. Molecular biology of breast cancer metastasis. Clinical implications of experimental studies on metastatic inefficiency. *Breast Cancer Res*. (2):400-407.

24. Friedl, P., and K. Wolf. 2003. Tumour-cell invasion and migration: diversity and escape mechanisms. *Nature reviews. Cancer*. 3(5):362–374.

25. Szabó, A. and R. Mayor. 2018. Mechanisms of Neural Crest Migration. *Annual review of genetics*. (52):43–63.

26. Friedl, P., J. Locker, E. Sahai, and J. E. Segall .2012. Classifying collective cancer cell invasion. *Nature cell biology*. 14(8):777–783.

27. Konen, J., E. Summerbell, B. Dwivedi, K. Galior, Y. Hou, L. Rusnak, A. Chen, J. Saltz, W. Zhou, L. H. Boise, P. Vertino, L. Cooper, K. Salaita, J. Kowalski, and A. I. Marcus. 2017. Image-guided genomics of phenotypically heterogeneous populations reveals vascular signalling during symbiotic collective cancer invasion. *Nature communications*. (8):15078.

28. Summerbell, E. R., J. K. Mouw, J. S. K. Bell, C. M. Knippler, B. Pedro, J. L. Arnst, T. O. Khatib, R. Commander, B. G. Barwick, J. Konen, B. Dwivedi, S. Seby, J. Kowalski, P. M. Vertino, and A. I. Marcus. 2020. Epigenetically heterogeneous tumor cells direct collective

invasion through filopodia-driven fibronectin micropatterning. *Science advances*. 6(30):eaaz6197.

29. Commander, R., C. Wei, A. Sharma, J. K. Mouw, L. J. Burton, E. Summerbell, D. Mahboubi, R. J. Peterson, J. Konen, W. Zhou, Y. Du, H. Fu, M. Shanmugam, and A. I. Marcus. 2020. Subpopulation targeting of pyruvate dehydrogenase and GLUT1 decouples metabolic heterogeneity during collective cancer cell invasion. *Nature communications*. 11(1):1533.
30. Zhang J., K. F. Goliwas, W. Wang, P. V. Taufalele, F. Bordeleau, and C. A. Reinhart-King. 2019. Energetic regulation of coordinated leader-follower dynamics during collective invasion of breast cancer cells. *Proc Natl Acad Sci U S A*. 116(16):7867-7872.
31. Nasr, M. M. and C. C. Lynch. 2023. How circulating tumor cluster biology contributes to the metastatic cascade: from invasion to dissemination and dormancy. *Cancer metastasis reviews*. 42(4):1133–1146.
32. Aceto, N., A. Bardia, D. T. Miyamoto, M. C. Donaldson, B. S. Wittner, J. A. Spencer, M. Yu, A. Pely, A. Engstrom, H. Zhu, B. W. Brannigan, R. Kapur, S. L. Stott, T. Shioda, S. Ramaswamy, D. T. Ting, C. P. Lin, M. Toner, D. A. Haber, and S. Maheswaran. 2014. Circulating tumor cell clusters are oligoclonal precursors of breast cancer metastasis. *Cell*. 158(5):1110–1122.
33. Cheung K. J. and A. J. Ewald. 2016. A collective route to metastasis: Seeding by tumor cell clusters. *Science.* (352):167-169.
34. Kanikarla-Marie, P., M. Lam, A. V. Sorokin, M. J. Overman, S. Kopetz and D. G. Menter. 2018. Platelet Metabolism and Other Targeted Drugs; Potential Impact on Immunotherapy. *Frontiers in oncology*. (8):107.

35. Liu, Q., Q. Liao and Y. Zhao. 2016. Myeloid-derived suppressor cells (MDSC) facilitate distant metastasis of malignancies by shielding circulating tumor cells (CTC) from immune surveillance. *Medical hypotheses*. (87):34–39.

36. Vuononvirta, J., F. M. Marelli-Berg and T. Poobalasingam. 2021. Metabolic regulation of T lymphocyte motility and migration. *Molecular aspects of medicine*. (77):100888.

37. Plotnikov S. V., A. M. Pasapera, B. Sabass and C. M. Waterman. 2012. Force fluctuations within focal adhesions mediate ECM-rigidity sensing to guide directed cell migration. *Cell*. (151):1513-1527.

38. Bear J. E. and J. M. Haugh. 2014. Directed migration of mesenchymal cells: where signaling and the cytoskeleton meet. *Curr Opin Cell Biol*. (30):74-82.

39. Wolf, K. and P. Friedl. 2009. Mapping proteolytic cancer cell-extracellular matrix interfaces. *Clinical & experimental metastasis*. 26(4):289–298. https://doi.org/10.1007/s10585-008-9190-2

40. Burk, J., A. Sassmann, C. Kasper, A. Nimptsch and S. Schubert. 2022. Extracellular Matrix Synthesis and Remodeling by Mesenchymal Stromal Cells Is Context-Sensitive. *International journal of molecular sciences*. 23(3):1758.

41. Pulyaeva H., J. Bueno, M. Polette, P. Birembaut, H. Sato, M. Seiki and E. W. Thompson. 1997. MT1-MMP correlates with MMP-2 activation potential seen after epithelial to mesenchymal transition in human breast carcinoma cells. *Clin Exp Metastasis*. (2):111-20. Erratum in: Clin Exp Metastasis 1997 May;15(3):338.

42. Itoh K., K. Yoshioka, H. Akedo, M. Uehata, T. Ishizaki and S. Narumiya. An essential part for Rho-associated kinase in the transcellular invasion of tumor cells. 1999. *Nat Med*. (2):221-5.

43. Friedl, P., S. Borgmann and E. B. Bröcker. 2001. Amoeboid leukocyte crawling through extracellular matrix: lessons from the Dictyostelium paradigm of cell movement. *Journal of leukocyte biology*. 70(4):491–509.

44. Lewis, W. H. 1934. On the locomotion of the polymorphonuclear neutrophiles of the rat in autoplasma cultures. *Bull. Johns Hopkins. Hosp*. (4):273–279.

45. Friedl P., K. S. Zänker, E. B. Bröcker. 1998. Cell migration strategies in 3-D extracellular matrix: differences in morphology, cell matrix interactions, and integrin function. *Microsc Res Tech*. 43(5):369-78.

46. Graziani V., I. Rodriguez-Hernandez, O. Maiques, and V. Sanz-Moreno. 2022. The amoeboid state as part of the epithelial-to-mesenchymal transition programme. *Trends Cell Biol*. 32(3):228-242.

47. Hanahan, D. and R. A. Weinberg. 2011. Hallmarks of cancer: the next generation. *Cell*. 144(5):646–674.

48. Lamouille, S., J. Xu and R. Derynck. 2014. Molecular mechanisms of epithelial-mesenchymal transition. *Nature reviews. Molecular cell biology*. 15(3):178–196.

49. Thiery J. P., H. Acloque, R. Y. Huang and M. A. Nieto. 2009. Epithelial-mesenchymal transitions in development and disease. *Cell.* (139):871-890.

50. Bakir, B., A. M. Chiarella, J. R. Pitarresi and A. K. Rustgi. 2020. EMT, MET, Plasticity, and Tumor Metastasis. *Trends in cell biology*. 30(10):764–776.

51. Pal, A., T. F. Barrett, R. Paolini, A. Parikh and S. V. Puram. 2021. Partial EMT in head and neck cancer biology: a spectrum instead of a switch. *Oncogene*. 40(32):5049–5065.

52. Aiello, N. M., R. Maddipati, R. J. Norgard, D. Balli, J. Li, S. Yuan, T. Yamazoe, T. Black, A. Sahmoud, E. E. Furth, D. Bar-Sagi and B. Z. Stanger. 2018. EMT Subtype Influences Epithelial Plasticity and Mode of Cell Migration. *Developmental cell*. 45(6):681–695.e4.

53. Alexandrova, A. Y., A. S. Chikina and T. M. Svitkina. 2020. Actin cytoskeleton in mesenchymal-to-amoeboid transition of cancer cells. *International review of cell and molecular biology*. (356):197–256.

54. Wolf, K., I. Mazo, H. Leung, K. Engelke, U. H. von Andrian, E. I. Deryugina, A. Y. Strongin, E. B. Bröcker and P. Friedl. 2003. Compensation mechanism in tumor cell migration: mesenchymal-amoeboid transition after blocking of pericellular proteolysis. *The Journal of cell biology*. 160(2):267–277.

55. Taddei, M. L., E. Giannoni, A. Morandi, L. Ippolito, M. Ramazzotti, M. Callari, P. Gandellini and P. Chiarugi. 2014. Mesenchymal to amoeboid transition is associated with stem-like features of melanoma cells. *Cell communication and signaling : CCS*. (12):24.

56. Sannino, G., A. Marchetto, T. Kirchner and T. G. P. Grünewald. 2017. Epithelial-to-Mesenchymal and Mesenchymal-to-Epithelial Transition in Mesenchymal Tumors: A Paradox in Sarcomas?. *Cancer research*. 77(17):4556–4561.

57. Sheng, W., G. Wang, D. P. La Pierre, J. Wen, Z. Deng, C. K. Wong, D. Y. Lee and B. B. Yang. 2006. Versican mediates mesenchymal-epithelial transition. *Molecular biology of the cell*. 17(4):2009–2020.

58. Aiello, N. M., R. Maddipati, R. J. Norgard, D. Balli, J. Li, S. Yuan, T. Yamazoe, T. Black, A. Sahmoud, E. E. Furth, D. Bar-Sagi and B. Z. Stanger. 2018. EMT Subtype Influences Epithelial Plasticity and Mode of Cell Migration. *Developmental cell*. 45(6):681–695.e4.

59. Yokoyama, S., H. Shigeishi, H. Murodumi, M. Sakuma, H. Kato, K. Higashikawa, K. Ohta, M. Sugiyama and M. Takechi. 2021. TGF-β1 induces amoeboid-to-mesenchymal transition of CD44high oral squamous cell carcinoma cells via miR-422a downregulation through ERK activation and Cofilin-1 phosphorylation. *Journal of oral pathology & medicine : official publication of the International Association of Oral Pathologists and the American Academy of Oral Pathology*. 50(2):155–164.

60. Dagogo-Jack, I., and A. T. Shaw. 2018. Tumour heterogeneity and resistance to cancer therapies. *Nature reviews. Clinical oncology*. 15(2):81–94.

61. Khatib, T. O., A. A. Amanso, C. M. Knippler, B. Pedro, E. R. Summerbell, N. M. Zohbi, J. M. Konen, J. K. Mouw, and A. I. Marcus. 2023. A live-cell platform to isolate phenotypically defined subpopulations for spatial multi-omic profiling. *PloS one*. 18(10):e0292554.

62. Bakhoum, S. F. and L. C. Cantley. 2018. The Multifaceted Role of Chromosomal Instability in Cancer and Its Microenvironment. *Cell*. 174(6):1347–1360.

63. Gee, M. E., Z. Faraahi, A. McCormick and R. J. Edmondson. 2018. DNA damage repair in ovarian cancer: unlocking the heterogeneity. Journal of ovarian research, 11(1), 50.

64. Pray, L. 2008. DNA Replication and Causes of Mutation. *Nature Education*. 1(1):214

65. Jackson, S. P. and J. Bartek. 2009. The DNA-damage response in human biology and disease. *Nature*. 461(7267):1071–1078.

66. Levine A. J. 1997. p53, the cellular gatekeeper for growth and division. *Cell*. 88(3):323–331.

67. Yoshida, K. and Y. Miki. 2004. Role of BRCA1 and BRCA2 as regulators of DNA repair, transcription, and cell cycle in response to DNA damage. *Cancer science*. 95(11):866–871.

68. Stewart-Morgan, K. R., N. Petryk and A. Groth. 2020. Chromatin replication and epigenetic cell memory. *Nature cell biology*. 22(4):361–371.

69. Mazor, T., A. Pankov, J. S. Song and J. F. Costello. 2016. Intratumoral Heterogeneity of the Epigenome. *Cancer cell*. 29(4):440–451.

70. McGranahan, N. and C. Swanton. 2017. Clonal Heterogeneity and Tumor Evolution: Past, Present, and the Future. *Cell*. 168(4):613–628.

71. Lawson, D. A., K. Kessenbrock, R. T. Davis, N. Pervolarakis and Z. Werb. 2018. Tumour heterogeneity and metastasis at single-cell resolution. *Nature cell biology*. 20(12):1349–1360.

72. Dhanyamraju, P. K., T. D. Schell, S. Amin and G. P. Robertson. 2022. Drug-Tolerant Persister Cells in Cancer Therapy Resistance. *Cancer research*. 82(14):2503–2514.

73. Lee, M. C., F. J. Lopez-Diaz, S. Y. Khan, M. A. Tariq, Y. Dayn, C. J. Vaske, A. J. Radenbaugh, H. J. Kim, B. M. Emerson and N. Pourmand. 2014. Single-cell analyses of transcriptional heterogeneity during drug tolerance transition in cancer cells by RNA sequencing. *Proceedings of the National Academy of Sciences of the United States of America*. 111(44):E4726–E4735.

74. Ilina, O., L. Campanello, P. G. Gritsenko, M. Vullings, C. Wang, P. Bult, W. Losert, and P. Friedl. 2018. Intravital microscopy of collective invasion plasticity in breast cancer. *Disease models & mechanisms*. 11(9):dmm034330.

75. Khalil, A. A., O. Ilina, P. G. Gritsenko, P. Bult, P. N. Span and P. Friedl. 2017. Collective invasion in ductal and lobular breast cancer associates with distant metastasis. *Clinical & experimental metastasis*. 34(6-7):421–429.

76. Henriet, E., H. Knutsdottir, E. M. Grasset, M. Dunworth, M. Haynes, J. S. Bader and A. J. Ewald. 2023. Triple negative breast tumors contain heterogeneous cancer cells expressing distinct KRAS-dependent collective and disseminative invasion programs. *Oncogene*. (42):737–747.

77. Rubenstein, D. and J. Kealey. 2010. Cooperation, Conflict, and the Evolution of Complex Animal Societies. *Nature Education Knowledge*. 3(10):78.

78. Barker, J. L., J. L. Bronstein, M. L. Friesen, E. I. Jones, H. K. Reeve, A. G. Zink and M. E. Frederickson. 2017. Synthesizing perspectives on the evolution of cooperation within and between species. *Evolution; international journal of organic evolution*. 71(4):814–825.

79. Clutton-Brock T. 2009. Cooperation between non-kin in animal societies. *Nature*. 462(7269):51–57.

80. Buatois, A. and M. Lihoreau. 2016. Evidence of trapline foraging in honeybees. *The Journal of experimental biology*. 219(Pt 16):2426–2429.

81. Ellis, S., Franks, D. W. and E. J. Robinson. 2014. Resource redistribution in polydomous ant nest networks: local or global?. *Behavioral ecology : official journal of the International Society for Behavioral Ecology*. 25(5):1183–1191.

82. Carter, G. G. and G. S. Wilkinson. 2015. Social benefits of non-kin food sharing by female vampire bats. *Proceedings. Biological sciences*. 282(1819):20152524.

83. Riehl, C. and M. E. Frederickson, M. E. 2016. Cheating and punishment in cooperative animal societies. *Philosophical transactions of the Royal Society of London. Series B, Biological sciences*. 371(1687):20150090.

84. Valencia-Aguilar, A., J. M. Guayasamin and C. P. A. Prado. 2021. Alloparental care in glassfrogs: males care for unrelated clutches only when associated with their own. *Scientific reports*. 11(1):1386.

85. Medzhitov R. 2007. Recognition of microorganisms and activation of the immune response. *Nature*. 449(7164):819–826.

86. Nedelcu A. M. 2020. The evolution of multicellularity and cancer: views and paradigms. *Biochemical Society transactions*. 48(4):1505–1518.

87. Campbell, N. R., A. Rao, M. V. Hunter, M. K. Sznurkowska, L. Briker, M. Zhang, M. Baron, S. Heilmann, M. Deforet, C. Kenny, L. P. Ferretti, T. H. Huang, S. Perlee, M. Garg, J. Nsengimana, M. Saini, E. Montal, M. Tagore, J. Newton-Bishop, M. R. Middleton, P. Corrie, D. J. Adams, R. Rabbie, N. Aceto, M. P. Levesque, R. A. Cornell, I. Yanai, J. B. Xavier, and R. M. White. 2021. Cooperation between melanoma cell states promotes metastasis through heterotypic cluster formation. *Developmental cell*. 56(20):2808–2825.e10.

88. Icard, P., P. Kafara, J. M. Steyaert, L. Schwartz and H. Lincet. 2014. The metabolic cooperation between cells in solid cancer tumors. *Biochimica et biophysica acta*. 1846(1):216–225.

89. Yang C., M. Cao, Y. Liu, Y. He, Y. Du, G. Zhang, and F. Gao. 2019. Inducible formation of leader cells driven by CD44 switching gives rise to collective invasion and metastases in luminal breast carcinomas. *Oncogene*. 38(46):7113-7132.

90. Waite, A. J., C. Cannistra and W. Shou. 2015. Defectors Can Create Conditions That Rescue Cooperation. *PLoS computational biology*. 11(12):e1004645.

91. Nagy, J. D., E. M. Victor and J. H. Cropper. 2007. Why don't all whales have cancer? A novel hypothesis resolving Peto's paradox. *Integrative and comparative biology*. 47(2):317–328.

92. Archetti M. 2021. Collapse of Intra-Tumor Cooperation Induced by Engineered Defector Cells. *Cancers*. 13(15):3674.

93. Geiman Q. M. 1964. COMPARATIVE PHYSIOLOGY: MUTUALISM, SYMBIOSIS, AND PARASITISM. *Annual review of physiology*. (26):75–108.

94. Zelmer D. A. 1998. An evolutionary definition of parasitism. *International journal for parasitology*. 28(3):531–533.

95. Poulin, R., & H. S. Randhawa. 2015. Evolution of parasitism along convergent lines: from ecology to genomics. *Parasitology*. 142 Suppl 1(Suppl 1):S6–S15.

96. Abel, L., A. Alcaïs and E. Schurr. 2014. The dissection of complex susceptibility to infectious disease: bacterial, viral and parasitic infections. *Current opinion in immunology*. (30):72–78.

97. Karsch-Bluman, A., A. Feiglin, E. Arbib, T. Stern, H. Shoval, O. Schwob, M. Berger and O. Benny. 2019. Tissue necrosis and its role in cancer progression. *Oncogene*. 38(11):1920–1935.

98. Cedervall, J., Y. Zhang and A. K. Olsson. 2016. Tumor-Induced NETosis as a Risk Factor for Metastasis and Organ Failure. *Cancer research*. 76(15):4311–4315.

99. Pan, Y., Y. Yu, X. Wang and T. Zhang. 2020. Tumor-Associated Macrophages in Tumor Immunity. *Frontiers in immunology*. (11):583084.

100. Mougi A. 2016. The roles of amensalistic and commensalistic interactions in large ecological network stability. *Scientific reports*. (6):29929.

101. Rooks, M. G. and W. S. Garrett. 2016. Gut microbiota, metabolites and host immunity. *Nature reviews. Immunology*. 16(6):341–352.

102. Martens, E. C., M. Neumann and M. S. Desai. 2018. Interactions of commensal and pathogenic microorganisms with the intestinal mucosal barrier. *Nature reviews. Microbiology*. 16(8):457–470.

103. Liu, Y., Y. Baba, T. Ishimoto, X. Gu, J. Zhang, D. Nomoto, K. Okadome, H. Baba and P. Qiu. 2022. Gut microbiome in gastrointestinal cancer: a friend or foe?. *International journal of biological sciences*. 18(10):4101–4117.

104. Meng, F., R. Li, L. Ma, L. Liu, X. Lai, D. Yang, J. Wei, D. Ma and Z. Li. 2019. Porphyromonas gingivalis promotes the motility of esophageal squamous cell carcinoma by activating NF-κB signaling pathway. *Microbes and infection*. 21(7):296–304.

105. Li, N., Y. Feng, Y. Hu, C. He, C. Xie, Y. Ouyang, S. C. Artim, D. Huang, Y. Zhu, Z. Luo, Z. Ge and N. Lu. 2018. Helicobacter pylori CagA promotes epithelial mesenchymal transition in gastric carcinogenesis via triggering oncogenic YAP pathway. *Journal of experimental & clinical cancer research : CR*. 37(1):280.

106. Cao, L., S. Zhu, H. Lu, M. Soutto, N. Bhat, Z. Chen, D. Peng, J. Lin, J. Lu, P. Li, C. Zheng, C. Huang and W. El-Rifai. 2022. Helicobacter pylori-induced RASAL2 Through Activation of Nuclear Factor-κB Promotes Gastric Tumorigenesis via β-catenin Signaling Axis. *Gastroenterology*. 162(6):1716–1731.e17.

107. Roulot, A., D. Héquet, J. M. Guinebretière, A. Vincent-Salomon, F. Lerebours, C. Dubot, and R. Rouzier. 2016. Tumoral heterogeneity of breast cancer. Hétérogénéité tumorale des cancers du sein. *Annales de biologie clinique*. 74(6):653–660.

108. Morris, L. G., N. Riaz, A. Desrichard, Y. Şenbabaoğlu, A. A. Hakimi, V. Makarov, J. S. Reis-Filho, and T. A. Chan. 2016. Pan-cancer analysis of intratumor heterogeneity as a prognostic determinant of survival. *Oncotarget*. 7(9):10051–10063.

109. Dentro, S. C., I. Leshchiner, K. Haase, M. Tarabichi, J. Wintersinger, A. G. Deshwar, K. Yu, Y. Rubanova, G. Macintyre, J. Demeulemeester, I. Vázquez-García, K. Kleinheinz, D. G. Livitz, S. Malikic, N. Donmez, S. Sengupta, P. Anur, C. Jolly, M. Cmero, D. Rosebrock, S.E. Schumacher, Y. Fan, M. Fittall, R. M. Drews, X. Yao, T. B. K. Watkins, J. Lee, M. Schlesner, H. Zhu, D. J. Adams, N. McGranahan, C. Swanton, G. Getz, P. C. Boutros, M. Imielinski, R. Beroukhim, S. C. Sahinalp, Y. Ji, M. Peifer, I. Martincorena, F. Markowetz, V. Mustonen, K. Yuan, M. Gerstung, P. T. Spellman, W. Wang, Q. D. Morris, D. C. Wedge, P. Van Loo, and PCAWG Evolution and Heterogeneity Working Group and the PCAWG Consortium. 2021. Characterizing genetic intra-tumor heterogeneity across 2,658 human cancer genomes. *Cell*. 184(8):2239–2254.e39.

110. Marusyk, A., M. Janiszewska, and K. Polyak. 2020. Intratumor Heterogeneity: The Rosetta Stone of Therapy Resistance. *Cancer cell*. 37(4): 471–484.

111. Alvarez-Elizondo, M. B., and D. Weihs. 2022. Breast cancer stem cells: mechanobiology reveals highly invasive cancer cell subpopulations. *Cellular and molecular life sciences : CMLS*. 79(3):134.

112. Te Boekhorst, V., and P. Friedl. 2016. Plasticity of Cancer Cell Invasion-Mechanisms and Implications for Therapy. *Advances in cancer research*. 132:209–264.

113. Lintz, M., A. Muñoz, and C. A. Reinhart-King. 2017. The Mechanics of Single Cell and Collective Migration of Tumor Cells. *Journal of biomechanical engineering*. 139(2):0210051–0210059.

114. Nagai, T., T. Ishikawa, Y. Minami, and M. Nishita. 2020. Tactics of cancer invasion: solitary and collective invasion. *Journal of biochemistry*. 167(4):347–355.

115. Cheung, K. J., E. Gabrielson, Z. Werb, and A. J. Ewald. 2013. Collective invasion in breast cancer requires a conserved basal epithelial program. *Cell*. 155(7):1639–1651.

116. Loza, A. J., S. Koride, G. V. Schimizzi, B. Li, S. X. Sun, and G. D. Longmore. 2016. Cell density and actomyosin contractility control the organization of migrating collectives within an epithelium. *Molecular biology of the cell*. 27(22):3459–3470.

117. Zhao, Q., M. Barclay, J. Hilkens, X. Guo, H. Barrow, J. M. Rhodes, and L. G. Yu. 2010. Interaction between circulating galectin-3 and cancer-associated MUC1 enhances tumour cell homotypic aggregation and prevents anoikis. *Molecular cancer*. 9:154.

118. Lo, H. C., Z. Xu, I. S. Kim, B. Pingel, S. Aguirre, S. Kodali, J. Liu, W. Zhang, A. M. Muscarella, S. M. Hein, A. S. Krupnick, J. R. Neilson, S. Paust, J. M. Rosen, H. Wang, and X. H. Zhang. 2020. Resistance to natural killer cell immunosurveillance confers a selective advantage to polyclonal metastasis. *Nature cancer*. 1(7):709–722.

119. Gao, Y., Z. Wang, Q. Hao, W. Li, Y. Xu, J. Zhang, W. Zhang, S. Wang, S. Liu, M. Li, X. Xue, W. Zhang, C. Zhang, and Y. Zhang. 2017. Loss of ERα induces amoeboid-like migration of breast cancer cells by downregulating vinculin. *Nature communications*. (8):14483.

120. Khalil, A. A., O. Ilina, A. Vasaturo, J. H. Venhuizen, M. Vullings, V. Venhuizen, A. Bilos, C. G. Figdor, P. N. Span, and P. Friedl. 2020. Collective invasion induced by an autocrine purinergic loop through connexin-43 hemichannels. *The Journal of cell biology*. 219(10):e201911120.

121. Barde I., P. Salmon, and D. Trono. 2010. Production and titration of lentiviral vectors. *Curr Protoc Neurosci*. Chapter 4:Unit 4.21.

122. Bolger, A. M., M. Lohse, and B. Usadel. 2014. Trimmomatic: a flexible trimmer for Illumina sequence data. *Bioinformatics (Oxford, England)*. 30(15):2114–2120.

123. Ewels, P., M. Magnusson, S. Lundin, and M. Käller. 2016. MultiQC: summarize analysis results for multiple tools and samples in a single report. *Bioinformatics (Oxford, England)*. 32(19):3047–3048.

124. Dobin, A., C. A. Davis, F. Schlesinger, J. Drenkow, C. Zaleski, S. Jha, P. Batut, M. Chaisson, and T. R. Gingeras. 2013. STAR: ultrafast universal RNA-seq aligner. *Bioinformatics (Oxford, England)*. 29(1):15–21.

125. Anders, S., P. T. Pyl, and W. Huber. 2015. HTSeq--a Python framework to work with high-throughput sequencing data. *Bioinformatics (Oxford, England)*. 31(2):166–169.

126. Love, M. I., W. Huber, and S. Anders. 2014. Moderated estimation of fold change and dispersion for RNA-seq data with DESeq2. *Genome biology*. 15(12):550.

127. Benjamini, Y., and Y. Hochberg. 1995. Controlling the False Discovery Rate: A Practical and Powerful Approach to Multiple Testing. *Journal of the Royal Statistical Society. Series B (Methodological)*. 57(1):289–300.

128. Anders, S., D. J. McCarthy, Y. Chen, M. Okoniewski, G. K. Smyth, W. Huber, and M. D. Robinson. 2013. Count-based differential expression analysis of RNA sequencing data using R and Bioconductor. *Nature protocols*. 8(9):1765–1786.

129. Zhou, W., T.J. Triche Jr, P.W. Laird, and H. Shen. 2018. SeSAMe: reducing artifactual detection of DNA methylation by Infinium BeadChips in genomic deletions. *Nucleic acids research*. 46(20):e123-e123.

130. Pidsley, R., C. C. Y. Wong, M. Volta, K. Lunnon, J. Mill, and L. C. Schalkwyk. 2013. A data-driven approach to preprocessing Illumina 450K methylation array data. *BMC genomics*. 14(1):1-10.

131. Tian, Y., T.J. Morris, A.P. Webster, Z. Yang, S. Beck, A. Feber, and A. E. Teschendorff. 2017. ChAMP: updated methylation analysis pipeline for Illumina BeadChips. *Bioinformatics (Oxford, England)*. 33(24):3982-3984.

132. Hicks, S.C., K. Okrah, J. N. Paulson, J. Quackenbush, R.A. Irizarry, and H. C. Bravo. 2018. Smooth quantile normalization. *Biostatistics*. 19(2):185-198.

133. Aryee, M.J., A.E. Jaffe, H. Corrada-Bravo, C. Ladd-Acosta, A.P. Feinberg, K. D. Hansen, and R. A. Irizarry. 2014. Minfi: a flexible and comprehensive Bioconductor package for the analysis of Infinium DNA methylation microarrays. *Bioinformatics (Oxford, England)*. 30(10):1363-1369.

134. Xu, Z., L. Niu, and J. A. Taylor. 2021. The ENmix DNA methylation analysis pipeline for Illumina BeadChip and comparisons with seven other preprocessing pipelines. *Clinical Epigenetics*. 13(1):216.

135. Soucek, S., Y. Zeng, D. L. Bellur, M. Bergkessel, K. J. Morris, Q. Deng, D. Duong, N. T. Seyfried, C. Guthrie, J. P. Staley, M. B. Fasken, and A. H. Corbett. 2016. The Evolutionarily-conserved Polyadenosine RNA Binding Protein, Nab2, Cooperates with Splicing Machinery to Regulate the Fate of pre-mRNA. *Molecular and cellular biology*. 36(21):2697–2714.

136. Seyfried, N. T., E. B. Dammer, V. Swarup, D. Nandakumar, D. M. Duong, L. Yin, Q. Deng, T. Nguyen, C. M. Hales, T. Wingo, J. Glass, M. Gearing, M. Thambisetty, J. C. Troncoso, D. H. Geschwind, J. J. Lah, and A. I. Levey. 2017. A Multi-network Approach

Identifies Protein-Specific Co-expression in Asymptomatic and Symptomatic Alzheimer's Disease. *Cell systems*. 4(1):60–72.e4.

137. Konen, J., S. Wilkinson, B. Lee, H. Fu, W. Zhou, Y. Jiang, and A. I. Marcus. 2016. LKB1 kinase-dependent and -independent defects disrupt polarity and adhesion signaling to drive collagen remodeling during invasion. *Molecular biology of the cell*. 27(7):1069–1084.

138. Debnath, J., S. K. Muthuswamy, and J. S. Brugge. 2003. Morphogenesis and oncogenesis of MCF-10A mammary epithelial acini grown in three-dimensional basement membrane cultures. *Methods (San Diego, Calif.)*. 30(3):256–268.

139. Meijering, E., O. Dzyubachyk, and I. Smal. 2012. Methods for cell and particle tracking. *Methods in enzymology*. 504:183–200.

140. Marinkovich M. P. 2007. Tumour microenvironment: laminin 332 in squamous-cell carcinoma. *Nature reviews. Cancer*. 7(5):370–380.

141. Padmanaban, V., I. Krol, Y. Suhail, B. M. Szczerba, N. Aceto, J. S. Bader, and A. J. Ewald. 2019. E-cadherin is required for metastasis in multiple models of breast cancer. *Nature*. 573(7774):439–444.

142. Hwang, P. Y., A. Brenot, A. C. King, G. D. Longmore, and S. C. George. 2019. Randomly Distributed K14+ Breast Tumor Cells Polarize to the Leading Edge and Guide Collective Migration in Response to Chemical and Mechanical Environmental Cues. *Cancer research*. 79(8):1899–1912.

143. Hwang, T. L., T. T. Changchien, C. C. Wang, and C. M. Wu. 2014. Claudin-4 expression in gastric cancer cells enhances the invasion and is associated with the increased level of matrix metalloproteinase-2 and -9 expression. *Oncology letters*. 8(3):1367–1371.

144. Chen, L., Y. Yao, L. Sun, J. Zhou, M. Miao, S. Luo, G. Deng, J. Li, J. Wang, and J. Tang. 2017. Snail Driving Alternative Splicing of CD44 by ESRP1 Enhances Invasion and Migration in Epithelial Ovarian Cancer. *Cellular physiology and biochemistry : international journal of experimental cellular physiology, biochemistry, and pharmacology*. 43(6):2489–2504.

145. Wu, B., C. Yu, B. Zhou, T. Huang, L. Gao, T. Liu, and X. Yang. 2017. Overexpression of TROP2 promotes proliferation and invasion of ovarian cancer cells. *Experimental and therapeutic medicine*. 14(3):1947–1952.

146. Nguyen, B. P., M. C. Ryan, S. G. Gil, and W. G. Carter. 2000. Deposition of laminin 5 in epidermal wounds regulates integrin signaling and adhesion. *Current opinion in cell biology*. 12(5):554–562.

147. Fujisaki, H., and S. Hattori. 2002. Keratinocyte apoptosis on type I collagen gel caused by lack of laminin 5/10/11 deposition and Akt signaling. *Experimental cell research*. 280(2):255–269.

148. Manohar, A., S. G. Shome, J. Lamar, L. Stirling, V. Iyer, K. Pumiglia, and C. M. DiPersio. 2004. Alpha 3 beta 1 integrin promotes keratinocyte cell survival through activation of a MEK/ERK signaling pathway. *Journal of cell science*. 117(Pt 18):4043–4054.

149. Zahir, N., J. N. Lakins, A. Russell, W. Ming, C. Chatterjee, G. I. Rozenberg, M. P. Marinkovich, and V. M. Weaver. 2003. Autocrine laminin-5 ligates alpha6beta4 integrin and activates RAC and NFkappaB to mediate anchorage-independent survival of mammary tumors. *The Journal of cell biology*. 163(6):1397–1407.

150. Carpenter, P. M., A. V. Dao, Z. S. Arain, M. K. Chang, H. P. Nguyen, S. Arain, J. Wang-Rodriguez, S. Y. Kwon, and S. P. Wilczynski. 2009. Motility induction in breast carcinoma by mammary epithelial laminin 332 (laminin 5). *Molecular cancer research : MCR*. 7(4):462–475.

151. Kumagai, Y., J. Nio-Kobayashi, S. Ishida-Ishihara, H. Tachibana, R. Omori, A. Enomoto, S. Ishihara, and H. Haga. 2019. The intercellular expression of type-XVII collagen, laminin-332, and integrin-β1 promote contact following during the collective invasion of a cancer cell population. *Biochemical and biophysical research communications*. 514(4):1115–1121.

152. Te Molder, L., J. M. de Pereda, and A. Sonnenberg. 2021. Regulation of hemidesmosome dynamics and cell signaling by integrin α6β4. *Journal of cell science*. 134(18):jcs259004.

153. Hwang, P. Y., J. Mathur, Y. Cao, J. Almeida, J. Ye, V. Morikis, D. Cornish, M. Clarke, S. A. Stewart, A. Pathak, and G. D. Longmore. 2023. A Cdh3-β-catenin-laminin signaling axis in a subset of breast tumor leader cells control leader cell polarization and directional collective migration. *Developmental cell*. 58(1):34–50.e9.

154. Okamoto, O., S. Bachy, U. Odenthal, J. Bernaud, D. Rigal, H. Lortat-Jacob, N. Smyth, and P. Rousselle. 2003. Normal human keratinocytes bind to the alpha3LG4/5 domain of unprocessed laminin-5 through the receptor syndecan-1. *The Journal of biological chemistry*. 278(45):44168–44177.

155. Baba, Y., K. I. Iyama, K. Hirashima, Y. Nagai, N. Yoshida, N. Hayashi, N. Miyanari, and H. Baba. 2008. Laminin-332 promotes the invasion of oesophageal squamous cell carcinoma via PI3K activation. *British journal of cancer*. 98(5):974–980.

156. Paine, S. K., S. Das, C. Bhattacharyya, N. K. Biswas, R. Rao, A. De, and A. Basu. 2022. Autosomal recessive inheritance of a novel missense mutation of ITGB4 for Epidermolysis-Bullosa pyloric-atresia: a case report. *Molecular genetics and genomics : MGG*. 297(6):1581–1586.

157. Chen, W., J. M. C. Gard, Y. Epshtein, S. M. Camp, J. G. N. Garcia, J. R. Jacobson, and A. E. Cress. 2022. Integrin Beta 4E Promotes Endothelial Phenotypic Changes and Attenuates Lung Endothelial Cell Inflammatory Responses. *Frontiers in physiology*. 13:769325.

158. Boussaha, M., A. Boulling, V. Wolgust, L. Bourgeois-Brunel, P. Michot, C. Grohs, N. Gaiani, P. Y. Grivaud, H. Leclerc, C. Danchin-Burge, M. Vilotte, J. Rivière, D. Boichard, J. M. Gourreau, and A. Capitan. 2023. Integrin alpha 6 homozygous splice-site mutation causes a new form of junctional epidermolysis bullosa in Charolais cattle. *Genetics, selection, evolution : GSE*. 55(1):40.

159. Mateo F., O. Meca-Cortés, T. Celià-Terrassa, Y. Fernández, I. Abasolo, L. Sánchez-Cid, R. Bermudo, A. Sagasta, L. Rodríguez-Carunchio, M. Pons, V. Cánovas, M. Marín-Aguilera, L. Mengual, A. Alcaraz, S. Schwartz Jr, B. Mellado, K. Y. Aguilera, R. Brekken, P.L. Fernández, R. Paciucci, T., and M. Thomson. 2014. SPARC mediates metastatic cooperation between CSC and non-CSC prostate cancer cell subpopulations. *Mol Cancer*. 13:237.

160. Kumamoto, C. A., M. S. Gresnigt, and B. Hube. 2020. The gut, the bad and the harmless: Candida albicans as a commensal and opportunistic pathogen in the intestine. *Current opinion in microbiology*. 56:7–15.

161. Yang, D., M. Zhang, C. Su, B. Dong, and Y. Lu. 2023. Candida albicans exploits N-acetylglucosamine as a gut signal to establish the balance between commensalism and pathogenesis. *Nature communications*. 14(1):3796.

162. Zheng, Y., R. L. Hunt, A. E. Villaruz, E. L. Fisher, R. Liu, Q. Liu, G. Y. C. Cheung, M. Li, and M. Otto. 2022. Commensal Staphylococcus epidermidis contributes to skin barrier homeostasis by generating protective ceramides. *Cell host & microbe*. 30(3):301–313.e9.

163. Fujiwara-Tani, R., S. Mori, R. Ogata, R. Sasaki, A. Ikemoto, S. Kishi, M. Kondoh and H. Kuniyasu. 2023. Claudin-4: A New Molecular Target for Epithelial Cancer Therapy. *International journal of molecular sciences*. 24(6):5494.

164. Cheung, K. J., V. Padmanaban, V. Silvestri, K. Schipper, J. D. Cohen, A. N. Fairchild, M. A. Gorin, J. E. Verdone, K. J. Pienta, J. S. Bader and A. J. Ewald. 2016. Polyclonal breast cancer metastases arise from collective dissemination of keratin 14-expressing tumor cell clusters. *Proceedings of the National Academy of Sciences of the United States of America*. 113(7):E854–E863.

165. Lavenus, S. B., S. M. Tudor, M. F. Ullo, K. W. Vosatka and J. S. Logue. 2020. A flexible network of vimentin intermediate filaments promotes migration of amoeboid cancer cells through confined environments. *The Journal of biological chemistry*. 295(19):6700–6709.

166. Sari, B., O. Gulbey and K. J. Hamill. 2023. Laminin 332 expression levels predict clinical outcomes and chemotherapy response in patients with pancreatic adenocarcinoma. *Frontiers in cell and developmental biology*. (11):1242706.

167. Gaiko-Shcherbak, A., G. Fabris, G. Dreissen, R. Merkel, B. Hoffmann and E. Noetzel. 2015. The Acinar Cage: Basement Membranes Determine Molecule Exchange and Mechanical Stability of Human Breast Cell Acini. *PloS one*. 10(12):e0145174.

168. Yang, L., L. Yong, X. Zhu, Y. Feng, Y. Fu, D. Kong, W. Lu and T. Y. Zhou. 2020. Disease progression model of 4T1 metastatic breast cancer. *Journal of pharmacokinetics and pharmacodynamics*. 47(1):105–116.